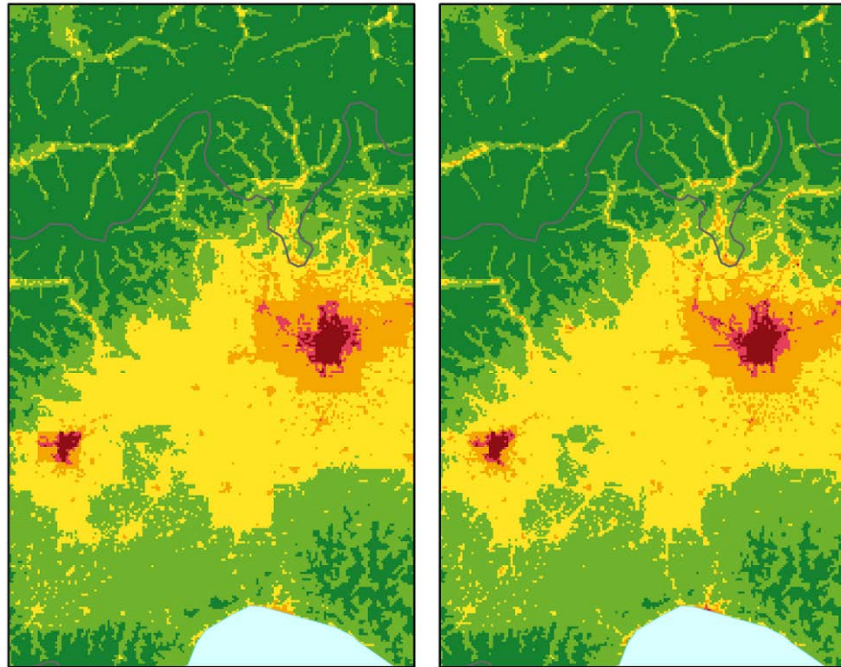


# Satellite data inclusion and kernel based potential improvements in NO<sub>2</sub> mapping



**ETC/ACM Technical Paper 2017/14**  
**April 2018**

*Jan Horálek, Peter de Smet, Philipp Schneider, Bino Maiheu,  
Frank de Leeuw, Stijn Janssen, Nina Benešová, Wouter Lefebvre*



The European Topic Centre on Air Pollution and Climate Change Mitigation (ETC/ACM) is a consortium of European institutes under contract of the European Environment Agency  
RIVM Aether CHMI CSIC EMISIA INERIS NILU ÖKO-Institut ÖKO-Recherche PBL UAB UBA-V VITO 4Sfera

**Front page picture:**

Concentration map of NO<sub>2</sub> annual average of 2010 using OMI satellite data and 'CHIMERE-SHERPA' (left) resp. 'CHIMERE-SHERPA with QUARK kernel method applied' (right) model outputs among supplementary data, 2010, western Po valley. Resolution: 1x1 km. Units: µg.m<sup>-3</sup>. (This paper, extracted from Map 4.3, centre and right map.)

**Author affiliation:**

Jan Horálek, Nina Benešová: Czech Hydrometeorological Institute (CHMI), Prague, Czech Republic

Peter de Smet, Frank de Leeuw: National Institute for Public Health and the Environment (RIVM), Bilthoven, The Netherlands

Philipp Schneider: Norwegian Institute of Air Research (NILU), Kjeller, Norway

Bino Maiheu, Stijn Janssen, Wouter Lefebvre: Flemish institute for technological research (VITO), Mol, Belgium

**DISCLAIMER**

This ETC/ACM Technical Paper has not been subjected to European Environment Agency (EEA) member country review. It does not represent the formal views of the EEA.

© ETC/ACM, 2017

ETC/ACM Technical Paper 2017/14

European Topic Centre on Air Pollution and Climate Change Mitigation

PO Box 1

3720 BA Bilthoven

The Netherlands

Phone +31 30 2748562

Fax +31 30 2744433

Email [etcacm@rivm.nl](mailto:etcacm@rivm.nl)

Website <http://acm.eionet.europa.eu/>

# Contents

<b>1</b>	<b>Introduction</b> .....	<b>5</b>
<b>2</b>	<b>Methodology</b> .....	<b>7</b>
2.1	Current method .....	7
2.2	Satellite data and QUARK kernel based model output inclusion.....	8
2.3	Uncertainty estimates of the concentration maps.....	8
<b>3</b>	<b>Input data</b> .....	<b>11</b>
3.1	Monitoring data .....	11
3.2	Chemical transport modelling data .....	12
3.3	Satellite data .....	14
3.4	Other supplementary data.....	16
<b>4</b>	<b>Analysis applying satellite data and QUARK kernel method</b> .....	<b>19</b>
4.1	Satellite data inclusion in mapping .....	19
4.2	Use of QUARK kernel based model output in mapping.....	23
4.2.1	<i>Comparison of modelling data with measurements</i> .....	23
4.2.2	<i>Inclusion of 'CHIMERE with QUARK applied' model output in mapping</i> .....	24
<b>5</b>	<b>Conclusion</b> .....	<b>35</b>
	<b>References</b> .....	<b>37</b>
<b>Annex 1</b>	<b>Overview of current and future satellite products of NO<sub>2</sub></b> .....	<b>39</b>
A1.1	Ozone Monitoring Instrument (OMI) .....	39
A1.2	GOME-2 onboard of the MetOp platform .....	40
A1.3	TROPOMI onboard of the Sentinel-5P platform .....	41
A1.4	Use of NO <sub>2</sub> satellite data in Copernicus Atmosphere Monitoring Service (CAMS) .....	41
	References .....	42
<b>Annex 2</b>	<b>QUARK kernel method and its potential integrating with ETC/ACM NO<sub>2</sub> mapping</b> .....	<b>43</b>
A2.1	QUARK kernel methodology description .....	43
A2.2	Potential integration of the QUARK kernel method in the ETC/ACM mapping methodology .....	47
A2.3	Potential alternative coupling of the QUARK kernel method with the ETC/ACM mapping methodology .....	49
A2.4	Discussion on the spatial resolution and its influence on the exposure assessment .....	50
A2.5	Potential research questions list.....	52
	References .....	53



# 1 Introduction

Air quality mapping is an important task in order to provide as most complete spatial information about the air quality in a given region as possible. Among air pollutants nitrogen dioxide (NO<sub>2</sub>) is of main relevance for the map production, together with PM and ozone, due to the health impacts connected with these pollutants. While annual European-wide maps for PM and ozone have been produced regularly for many years under ETC/ACM, NO<sub>2</sub> maps have been added to the set of regular maps just recently (Horálek et al., 2017a). In all cases, the mapping method is based primarily on air quality measurements. It combines monitoring data, chemical transport model results and other supplementary data in the data fusion by linear regression model followed by kriging of its residuals ('residual kriging'). The rural and urban areas are mapped separately with a subsequent merging of these map layers. The method can be described as the *regression – interpolation – merging mapping*.

Under Horálek et al. (2017b), an improved NO<sub>2</sub> mapping methodology was developed through inclusion of land cover and road data, together with other supplementary variables. Next to this, the urban traffic air quality is taken into account as an additional map layer included in the merging process at this improved method. All the map layers are created on a grid at 1x1 km<sup>2</sup> resolution. For population exposure calculations we go even inside this 1x1 km<sup>2</sup> grid in order to better reflect the population exposed to traffic. This improved method for NO<sub>2</sub> has already been incorporated in the annual routine mapping (Horálek et al., 2017c, 2018).

In this paper, two new data sources are examined to assess their potential contribution to methodological improvements for NO<sub>2</sub> mapping under ETC/ACM. The first is the inclusion of satellite data. The second is the data output from the model using the so called 'QUARK kernel method'.

- *Satellite data* is now widely used in regional mapping of PM and NO<sub>2</sub>, thanks to data assimilation techniques. Earlier, the suitability of the satellite OMI based product for the spatial mapping of NO<sub>2</sub> was tested (Schneider et al, 2012). In this earlier study, it was recommended to investigate the use of the OMI based NO<sub>2</sub> high resolution products in the operational ETC/ACM air quality mapping methodology. Based on this recommendation, we examine now whether this OMI based satellite imagery data can improve the operational NO<sub>2</sub> mapping as a supplementary data source in the routine methodology.
- The *QUARK kernel method* has been developed in a recent DG-ENV project<sup>1</sup> as a downscaling methodological tool to improve air quality modelling that is used for EU-wide NO<sub>2</sub> exposure assessment. This paper examines the use of the QUARK kernel based model output in the ETC/ACM mapping. For doing this, we examine and mutually compare the use of two model outputs in the ETC/ACM mapping, namely the 'CHIMERE-SHERPA' model output in 7 x 7 km<sup>2</sup> resolution and the 'CHIMERE-SHERPA with QUARK kernel method applied' model output in 125 x 125 m<sup>2</sup> that is aggregated into a 1x1 km<sup>2</sup> resolution.

Chapter 2 describes the methodological aspects. Chapter 3 documents input data. Chapter 4 presents the analysis and results of the examination of the application of both satellite data and QUARK application based model output in the mapping methodology. Chapter 5 discusses the results and summarizes the conclusions.

---

<sup>1</sup> Service contract 070201/2015/SER/717473/C.3 for DG-ENV – Improved Tools for Assessing NO<sub>2</sub> Exposure. Project team: VITO (Belgium), King's College (UK).

Annex 1 presents an overview of the current and future NO<sub>2</sub> satellite products and gives a brief summary of the use of NO<sub>2</sub> satellite data in the Copernicus Atmospheric Monitoring Service (CAMS). Annex 2 describes the QUARK kernel method, which performs a downscaling on coarser resolution background concentration maps, and discusses its potential integration with the ETC/ACM mapping methodology. Next to the use of the QUARK kernel based model output as a proxy in the ETC/ACM mapping (as examined in a main report), an alternative potential coupling of the QUARK method with the ETC/ACM mapping methodology is discussed.

## 2 Methodology

### 2.1 Current method

The current mapping methodology used by ETC/ACM to create the NO<sub>2</sub> concentration maps is described in Horálek et al. (2017b). It is an improved variant of the *regression – interpolation – merging mapping* method. Separate map layers are created for rural, urban background and urban traffic areas on a grid at 1x1 km<sup>2</sup> resolution. The rural background map layer is based on the rural background stations, the urban background map layer on the urban and the suburban background stations, and the urban traffic map layer on the urban and the suburban traffic stations. All the map layers are created using a linear regression model followed by kriging of the residuals produced from that model (residual kriging). Interpolation is therefore carried out according to the relation:

$$\hat{Z}(s_0) = c + a_1 \cdot X_1(s_0) + a_2 \cdot X_2(s_0) + \dots + a_n \cdot X_n(s_0) + \eta(s_0) \quad (2.1)$$

where  $\hat{Z}(s_0)$  is the estimated value of the air pollution indicator at the point  $s_0$ ,  
 $X_1(s_0), X_2(s_0), \dots, X_n(s_0)$  are the  $n$  number of individual supplementary variables at the point  $s_0$ ,  
 $c, a_1, a_2, \dots, a_n$  are the  $n+1$  parameters of the linear regression model estimated based on the observed values and supplementary data at the points of measurement,  
 $\eta(s_0)$  is the spatial interpolation of the residuals of the linear regression model at the point  $s_0$  estimated based on the residuals at the points of measurement.

The spatial interpolation of the regression's residuals is carried out using ordinary kriging, according to

$$\hat{\eta}(s_0) = \sum_{i=1}^N \lambda_i \eta(s_i) \quad \text{with} \quad \sum_{i=1}^N \lambda_i = 1, \quad (2.2)$$

where  $\hat{\eta}(s_0)$  is the interpolated value at a point  $s_0$ , derived from the residuals of the linear regression model at the points of measurement  $s_i, i = 1, \dots, N$ ,  
 $\eta(s_i)$  are the residuals of the linear regression model at  $N$  points of measurement  $s_i, i = 1, \dots, N$ ,  
 $\lambda_1, \dots, \lambda_N$  are the estimated weights based on the variogram, which is a measure of a spatial correlation, see Cressie (1993).

For different map layers (rural background, urban background, and urban traffic) different supplementary data are used, depending on their improvement to the fit of the regression. The three map layers are merged into one final map using a weighting procedure:

$$\hat{Z}_F(s_0) = (1 - w_U(s_0)) \cdot \hat{Z}_R(s_0) + w_U(s_0)(1 - w_T(s_0)) \cdot \hat{Z}_{UB}(s_0) + w_U(s_0)w_T(s_0) \cdot \hat{Z}_T(s_0) \quad (2.3)$$

where  $\hat{Z}_F(s_0)$  is the resulting estimated concentration in a grid cell  $s_0$  for the final map,  
 $\hat{Z}_{UB}(s_0)$  is the estimated concentration in a grid cell  $s_0$  for the urban background map layer,  
 $\hat{Z}_R(s_0)$  is the estimated concentration in a grid cell  $s_0$  for the rural background map layer,  
 $\hat{Z}_T(s_0)$  is the estimated concentration in a grid cell  $s_0$  for the urban traffic map layer,  
 $w_U(s_0)$  is the weight representing the ratio of the urban character of the grid cell  $s_0$ ,

$w_T(s_0)$  is the weight representing the ratio of areas exposed to traffic air quality in the grid cell  $s_0$ .

The weight  $w_U(s_0)$  is based on the population density grid, while  $w_T(s_0)$  is based on the buffers around the roads.

For further details and for supplementary data used, see Horálek et al. (2007, 2017b).

## 2.2 Satellite data and QUARK kernel based model output inclusion

In this paper, we examine the inclusion of satellite data in the mapping as an additional supplementary variable  $X_i$  of Equation 2.1, in all map layers resp. areas.

Next to this, we also examined the improvement brought by the integration of the QUARK kernel method with the chemical transport model output, applied as supplementary data source in the linear regression and interpolation of the regression residuals. In the analysis, alternative model outputs (see Section 3.2) are used in Equation 2.1 instead of the routinely applied EMEP model output.

In some cases, the supplementary variables of Equation 2.1 are selected through a stepwise regression and backwards elimination of the weakest performing variables (Horálek et al., 2007). In this selection two criteria are applied in general, similar to Beelen et al. (2009): a variable is not excluded from the regression model that (i) increases the adjusted  $R^2$  value by more than 1%, and (ii) has a coefficient that conforms to the pre-specified direction of association between the variable and the pollutant.

## 2.3 Uncertainty estimates of the concentration maps

The uncertainty estimation of the mapping results is based on the ‘leave one out’ *cross-validation* method. It computes the quality of the spatial interpolation for each measurement point from all available information except from the point in question, i.e. it withholds one data point and then makes a prediction at the spatial location of that point. This procedure is repeated for all measurement points in the available set. The results of the cross-validation are expressed by statistical indicators and scatter plots. The main indicators used are *root mean squared error* (RMSE) and *bias*:

$$RMSE = \sqrt{\frac{1}{N} \sum_{i=1}^N (\hat{Z}(s_i) - Z(s_i))^2} \quad Bias = \frac{1}{N} \sum_{i=1}^N (\hat{Z}(s_i) - Z(s_i)) \quad (2.10)$$

where  $Z(s_i)$  is the observed air quality indicator value at the  $i^{\text{th}}$  point,  
 $\hat{Z}(s_i)$  is the estimated air quality indicator value at the  $i^{\text{th}}$  point using other information, except the observed indicator value at the  $i^{\text{th}}$  point,  
 $N$  is the number of the observational points.

Next to the RMSE expressed in absolute units, one could express this uncertainty in percentage by relating the RMSE to the mean of the air quality indicator value for all stations:

$$RRMSE = \frac{RMSE}{\frac{1}{N} \sum_{i=1}^N Z(s_i)} \cdot 100 \quad (2.11)$$

where  $RRMSE$  is the relative RMSE, expressed as percentage.

Other cross-validation indicators are the coefficient of determination  $R^2$  and the regression equation parameters *slope* and *intercept*, following from the scatter plot between the cross-validation predicted and the observed concentrations.

Next to the cross-validation, in some cases also the simple *comparison of measured and predicted grid values* was done. In these cases, the similar statistical indicators as in cross-validation are used (i.e. *RMSE, bias,  $R^2$ , slope* and *intercept*).



## 3 Input data

### 3.1 Monitoring data

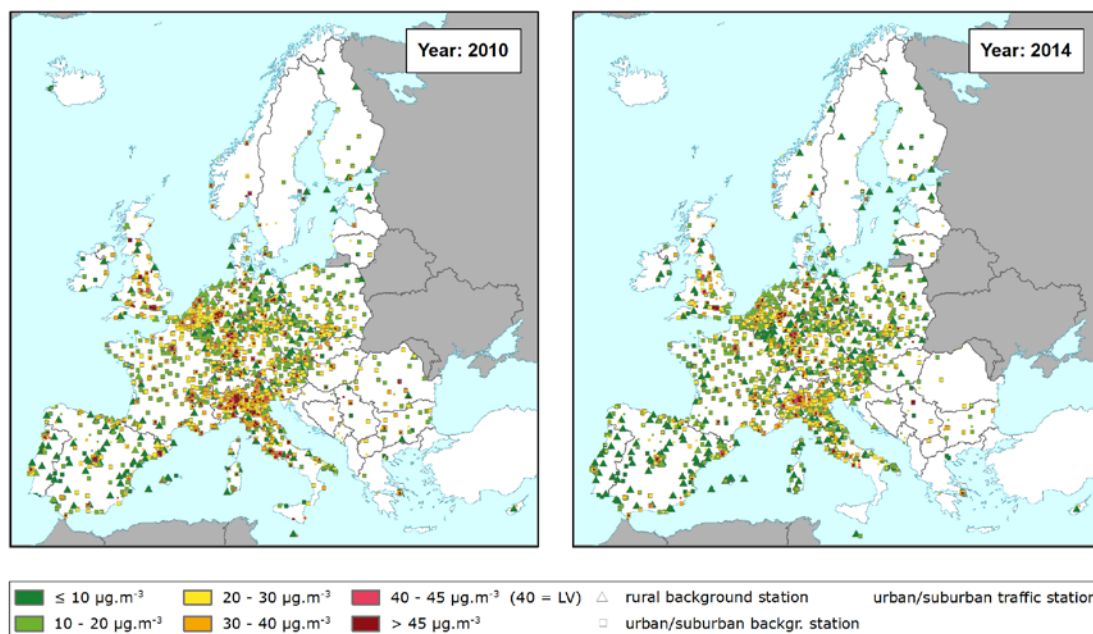
We extracted and applied the monitoring data for the year 2014 as this was the most up-to-date year with all data needed (monitoring, modelling, meteorology, satellite) available when this study started. Furthermore, we extracted the monitoring data for 2010 to allow for comparability with the QUARK kernel methodical calculation results already produced within the EU project and readily available to apply within our exploration of mapping improvement.

Air quality station monitoring data for the year 2010 is extracted from the *Air Quality e-Reporting database*, EEA (2017). Air quality station monitoring data for the year 2014 is extracted from the Air Quality e-Reporting database, EEA (2016a). This data set is supplemented with 11 additional rural background stations from the database EBAS (NILU, 2016) not reported to the Air Quality e-Reporting database, in agreement with Horálek et al. (2017c), in order to increase data coverage. Only data from stations classified by the Air Quality e-Reporting database and/or EBAS of the type *background* and *traffic* for the areas *rural*, *suburban* and *urban* are used. Station type *industrial* is not considered; it represents local scale concentration levels not applicable at the mapping resolution and information employed. The following pollutant and its indicator is considered:

NO<sub>2</sub> – annual average [ $\mu\text{g}\cdot\text{m}^{-3}$ ], years 2010 and 2014

Only the stations with annual data coverage of at least 75 percent are used. We excluded the stations outside the EEA map extent *Map\_1c* (EEA, 2011), which contains the mapping window of Map 3.1.

**Map 3.1 Station monitoring data, NO<sub>2</sub> annual average, 2010 (left) and 2014 (right)**



In total, 362 (for 2010) resp. 410 (for 2014) rural background stations, 1156 resp. 1126 urban/suburban background stations and 811 resp. 704 urban/suburban traffic stations are used. Rural traffic stations are not considered due to their small number (i.e. 16 in both years), in agreement with Horálek et al. (2017b). Map 3.1 shows the distribution of the selected stations by type and by annual average NO<sub>2</sub> concentration class.

### 3.2 Chemical transport modelling data

#### EMEP MSC-W

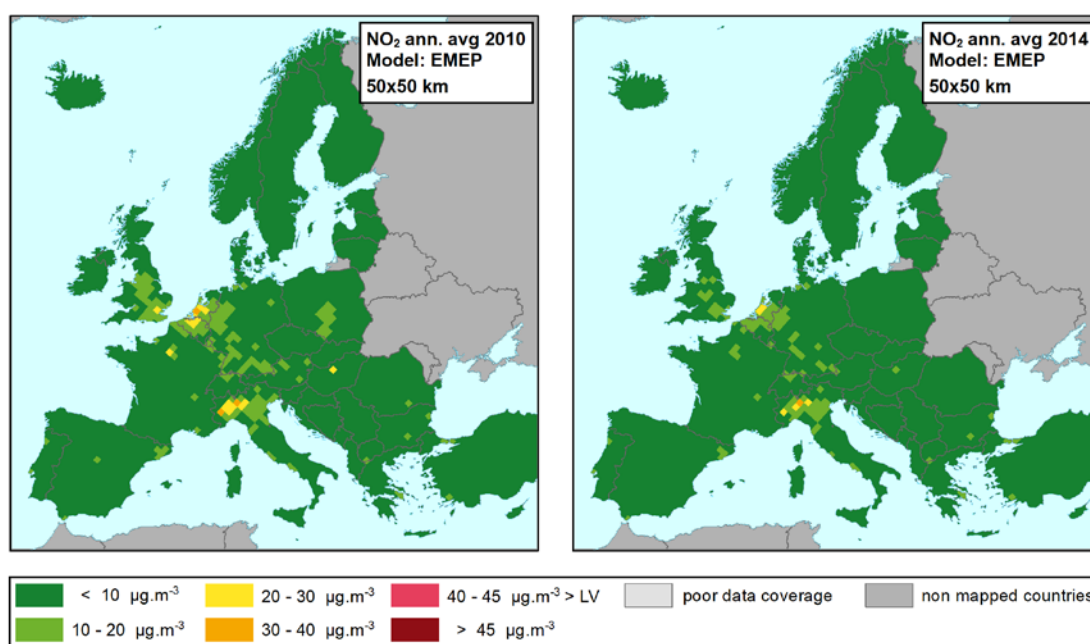
The EMEP MSC-W (formerly called Unified EMEP) model (version rv4.9) is an Eulerian chemical transport model. Simpson et al. (2012) and [https://wiki.met.no/emep/page1/emepmscw\\_opensource](https://wiki.met.no/emep/page1/emepmscw_opensource) (web site of Norwegian Meteorological Institute) describes the model in more detail. Emissions for the years 2010 (Mareckova et al., 2012) and 2014 (Mareckova et al., 2016) are used and the model is driven by ECMWF meteorology for each year 2010 and 2014. EMEP (2012, 2016) provide details on the EMEP modelling parametrisations for 2010 and 2014. The resolution of the model is about 50x50 km<sup>2</sup>. The parameters used are the same as for the monitoring data, i.e.

NO<sub>2</sub> – annual average [ $\mu\text{g}\cdot\text{m}^{-3}$ ], years 2010 and 2014

We downloaded the EMEP data from NMI (2016) in the form of NO<sub>2</sub> daily means. We aggregated this primary data to the NO<sub>2</sub> annual average 2010 and 2014 values.

Map 3.2 presents the ‘EMEP’ model outputs for 2010 and 2014.

**Map 3.2 EMEP model output, NO<sub>2</sub> annual average, 2010 (left) and 2014 (right)**



#### CHIMERE as used in SHERPA tool

The CHIMERE chemistry transport model (<http://www.lmd.polytechnique.fr/chimere>) is used, as it was derived in the context of the SHERPA project (<http://aqm.jrc.ec.europa.eu/sherpa.aspx>)<sup>2</sup>. The emissions are derived using EC4MACS proxies as used in the SHERPA emission database applied on GAINS total emissions at 2010 (total per country-pollutant-macrosector), see Bessagnet et al. (2012). Meteorology from the ECMWF-IFS model at 12.5x12.5 km<sup>2</sup> resolution is used. The original

<sup>2</sup> The background NO<sub>2</sub> concentration at 7 km used in the present report as well as underlying emissions were originally produced by INERIS with the CHIMERE under contract JRC/IPR/2014/H.2/0008/NC with the European Commission.

resolution of the model is  $0.125^\circ \times 0.0625^\circ$  (i.e. about  $7 \times 7 \text{ km}^2$ ). We refer further to this model as ‘CHIMERE-SHERPA’ or simply ‘CHIMERE’. The parameter used is

$\text{NO}_2$  – annual average [ $\mu\text{g.m}^{-3}$ ], year 2010

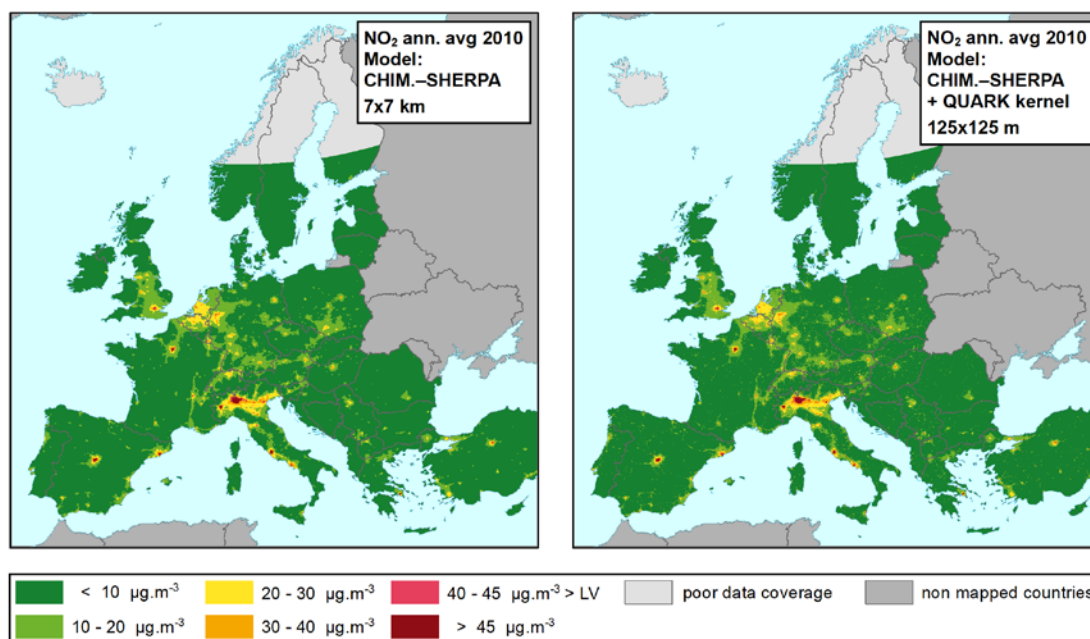
### CHIMERE as used in SHERPA tool, with QUARK kernel method applied

The QUARK kernel method (see Annex 2, Section A2.1) performs a downscaling of originally coarser resolution background concentration maps using dispersion kernels calculated by the IFDM model (Lefebvre, 2013). In our examinations we use the CHIMERE model as applied in SHERPA tool with application of this kernel method, as was derived by VITO under the DG-ENV project “Improved Tools for Assessing  $\text{NO}_2$  Exposure” for the year 2010. We refer further to this model as ‘CHIMERE-SHERPA with QUARK applied’ or simply ‘CHIMERE+QUARK’. The resolution of this data is  $125 \times 125 \text{ m}^2$ : the QUARK kernel method adds a traffic contribution in this fine resolution on top of a coarse ( $7 \times 7 \text{ km}^2$ ) background concentration. The parameter used is

$\text{NO}_2$  – annual average [ $\mu\text{g.m}^{-3}$ ], year 2010

Map 3.3 presents the ‘CHIMERE-SHERPA’ and the ‘CHIMERE-SHERPA with QUARK applied’ model outputs. One can see that the central and northern parts of Scandinavia and Iceland are not included in the CHIMERE domain. The covered domain is  $\langle -10.5^\circ, 37.5^\circ \rangle, \langle 34^\circ, 62^\circ \rangle$ .

**Map 3.3** ‘CHIMERE-SHERPA’ (left) and ‘CHIMERE-SHERPA with QUARK applied’ (right) model outputs,  $\text{NO}_2$  annual average, 2010

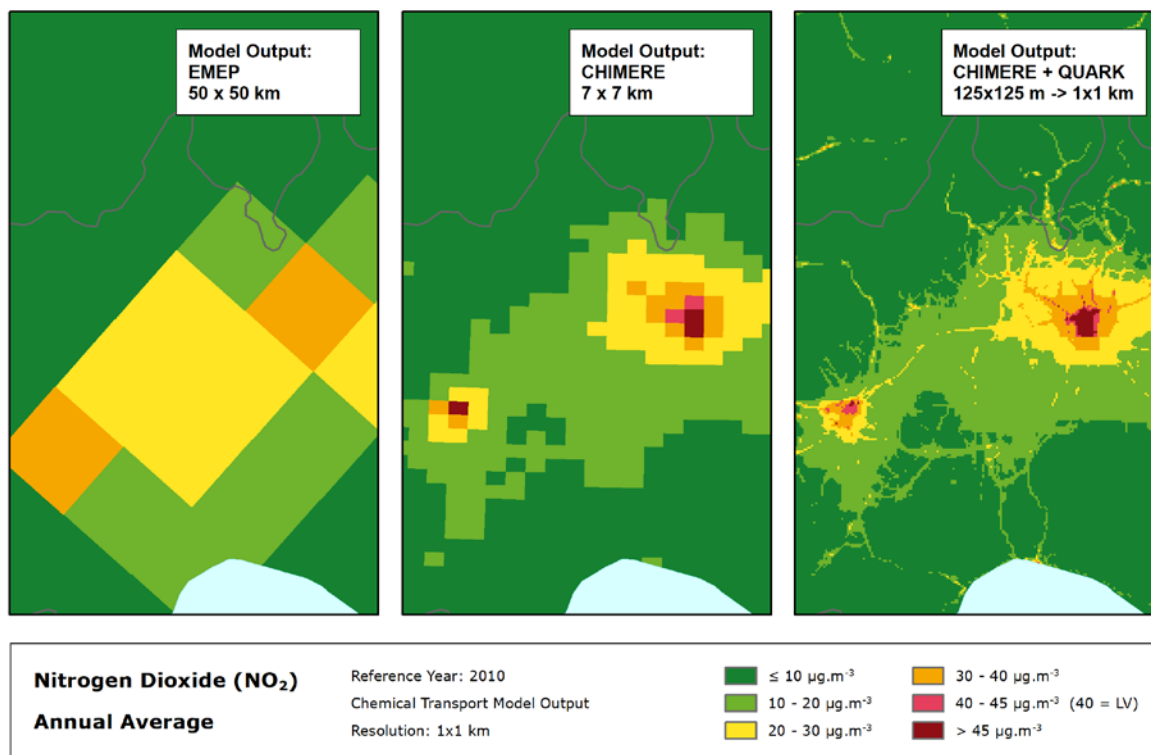


In order to better visualize the differences among the three models, Map 4.3 shows an extract of the three model output covering the western Po valley.

The ‘EMEP’ and the ‘CHIMERE-SHERPA’ model outputs were converted into ETRS89-LAEA5210 projection. The ‘CHIMERE-SHERPA with QUARK applied’ model outputs were provided already in ETRS89-LAEA5210 (resp. EPSG3035) projection. All model outputs were transformed into the reference EEA  $1 \times 1 \text{ km}^2$  grid: both ‘EMEP’ and ‘CHIMERE-SHERPA’ model outputs were imported into *ArcGIS* as a point shapefile, subsequently converted into a  $100 \times 100 \text{ m}^2$  raster grid (in order to minimize a distortion during the conversion) and then spatially aggregated into the  $1 \times 1 \text{ km}^2$  raster

grid; the 'CHIMERE-SHERPA with QUARK applied' data was spatially aggregated into the 1x1 km<sup>2</sup> grid.

**Map 3.4** EMEP (left), 'CHIMERE-SHERPA' (middle) and 'CHIMERE-SHERPA with QUARK applied' (right) model outputs, NO<sub>2</sub> annual average, 2010, western Po valley



### 3.3 Satellite data

Annual average NO<sub>2</sub> datasets for the years 2010 and 2014 were constructed from data acquired by the OMI instrument onboard the Aura platform, see Map 3.5. The parameter used is

NO<sub>2</sub> – annual average tropospheric vertical column density (VCD) [number of NO<sub>2</sub> molecules per cm<sup>2</sup> of earth surface], years 2010, 2014

The OMNO2d product generated by NASA was used as a basis, NASA (2017). While the product contains the column amounts of both the troposphere and the entire atmosphere, only the tropospheric column was used here. OMNO2d is a Level-3 daily global gridded OMI dataset that is derived from the Level-2 HDF-EOS5 files containing the swath data for each overpass. All the orbits within a given day (typically observed between 13:00 and 14:00 local time) are mapped into a 0.25x0.25 degrees grid, where the grid values are calculated using areal weighted interpolation of the original swath-level pixels.

A script in the R programming language (see <http://www.r-project.org>) was written to carry out the averaging of the data to an annual average grid. The set of 365 daily OMNO2d products was averaged over time to result in the annual average NO<sub>2</sub> datasets for 2010 and 2014. It should be noted that the daily products represent early afternoon values (see above), so the annual mean in fact represent the annual mean of the afternoon values. Next to this, it should be noted that no gap filling was carried out to handle gaps due to clouds. Instead, the averaging algorithm only used the available valid (cloud-free) values for each grid cell and ignored missing values. While this procedure has the

advantage that the annual mean cannot be subject to averaging errors caused by erroneous and often scientifically questionable gap-filling of large areas through spatial interpolation, it means on the other hand that the annual average estimates for some grid cells are calculated from significantly less than 365 values (for the most of Europe even significantly less than 274 days corresponding to 75% coverage, i.e. the minimum requirement on ground monitoring data) and that the number of daily observations going into the calculation of the mean varies from pixel to pixel (see Map 3.6). As such, some pixels and regions can be subject to biases and larger random errors. Spatially, this effect can sometimes result in increased “noise”, particularly in very cloudy regions.

**Figure 3.5 Annual average tropospheric column (VCD) of NO<sub>2</sub> for 2010 (left) and 2014 (right) as derived from OMI OMNO2d Level-3 daily product. Units: number of NO<sub>2</sub> molecules per cm<sup>2</sup>.**

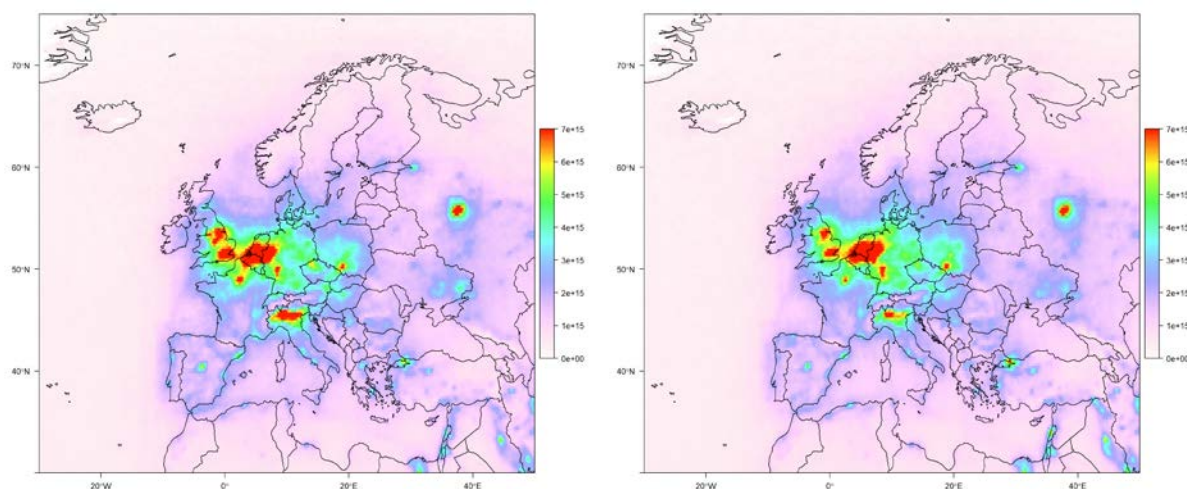
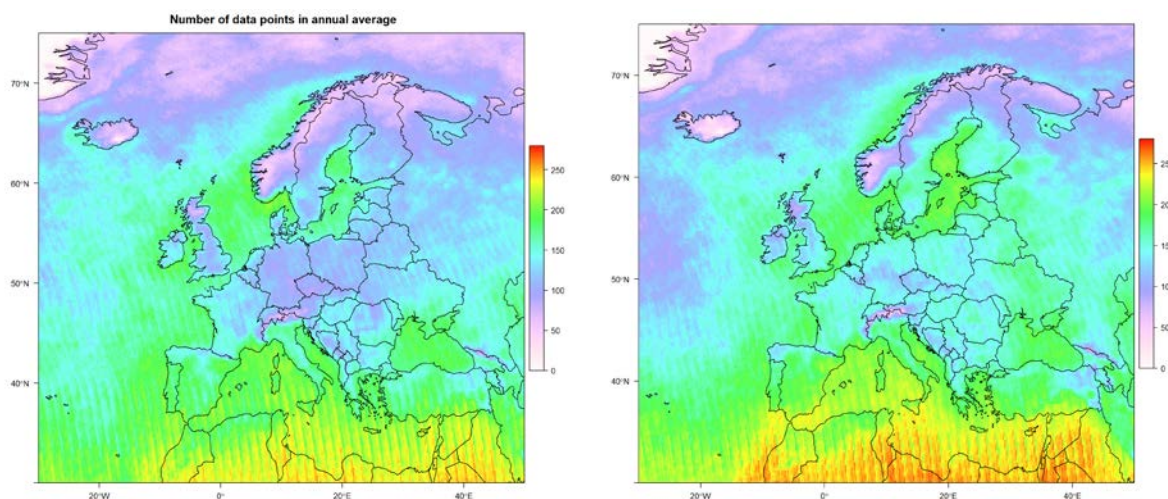


**Figure 3.6 Number of valid daily NO<sub>2</sub> observations in 2010 (left) and 2014 (right) that went into the calculation of the annual mean. Units: total number of daily OMI OMNO2d product files used for each pixel.**



The resulting annual global average NO<sub>2</sub> datasets for the years 2010 and 2014 were then cropped for the European domain (-30 to +50 degrees longitude, +30 to +75 degrees latitude) and subsequently projected from a simple latitude/longitude grid to the Lambert Equal Area projection. Finally, the data were converted to ArcGIS and spatially transformed into the reference EEA 1x1 km grid, similarly like the modelled data (see Section 3.2).

### 3.4 Other supplementary data

#### Land cover

CORINE Land Cover 2006 – grid 100 x 100 m<sup>2</sup>, Version 18.5 (09/2016) is used (EEA, 2016b). The country missing in this database is Andorra; the areas missing are Faroe Islands and Jan Mayen.

In order to reduce the high number of degrees of freedom in the CORINE Land Cover description, the 44 CLC classes (<http://www.eea.europa.eu/data-and-maps/data/clc-2006-vector-data-version-3/corine-land-cover-2006-classes>) have been re-grouped into the 8 more general classes in agreement with the recommendations of Horálek et al. (2017b), i.e. similarly like in Beelen et al. (2013).

**Table 3.1 Definition of general land cover classes, based on CLC2006 classes**

Label	General class description	CLC classes grid codes	CLC classes codes	CLC classes description
HDR	High density residential areas	1	111	Continuous urban fabric
LDR	Low density residential areas	2	112	Discontinuous urban fabric
IND	Industry	3, 7 – 9	121, 131 – 133	Industrial or commercial units, Mineral extraction sites, Dump sites, Construction sites
TRAF	Traffic	4 – 6	122 – 124	Road and rail networks and associated land, Ports, Airports
UGR	Urban green	10 – 11	141 – 142	Artificial, non-agricultural vegetated areas
AGR	Agricultural areas	12 – 22	211 – 244	Agricultural areas
NAT	Natural areas	23 – 34	311 – 335	Forest and semi natural areas
OTH	Other areas	35 – 44	411 – 523	Wetlands, Water bodies

Like in Horálek et al. (2017b), two aggregations are used, i.e. into 1x1 km<sup>2</sup> grid and into the circle with radius of 5 km, as a floating average for all 1x1 km<sup>2</sup> grid cells. The reason for these two aggregations is this: 1x1 km is directly related to the mapping and calculation resolution, the circle with radius of 5 km corresponds to a buffer of 5 km often used in LUR models (Hoek et al., 2008). For each general CLC class we spatially aggregated the high land use resolution into the 1x1 km<sup>2</sup> EEA standard grid resolution. The aggregated grid square value represents for each general class the total area of this class as percentage of the total 1x1 km<sup>2</sup> square area. For the floating averaging of the circle with radius 5 km around all relevant 1x1 km<sup>2</sup> grid cells, the aggregated grid square value represents for each general class the total area of this class as percentage of the total area of this circle (which is 8.1 square kilometers; this value is influenced by the 100x100 m<sup>2</sup> resolution of the land cover data).

In the analysis, the first seven classes have been used only, while the class OTH has been omitted as redundant, as it can be expressed by the other general classes: the percentage of the grid square area attributed to this class can be calculated by subtracting the percentages attributed to other seven classes from 100.

#### Altitude

We use the altitude data field (in m) of *Global Multi-resolution Terrain Elevation Data 2010 (GMTED2010)*, with an original grid resolution of 15x15 arcseconds coming from U.S. Geological Survey Earth Resources Observation and Science, see Danielson et al. (2011). The data were converted into the ETRS89-LAEA5210 projection, resampled to 100x100 m resolution, shifted to the extent of EEA reference grid, and spatially aggregated into 1x1 km<sup>2</sup> grid resolution.

Next to this, another aggregation has been executed based on the 1x1 km<sup>2</sup> grid cells, i.e. the floating averaging of the circle with *radius of 5 km* around all relevant grid cells.

### Meteorological data

The meteorological parameters used are *wind speed* (annual average for 2014, in m.s<sup>-1</sup>) and *surface net solar radiation* (annual average of daily sum for 2014, MWs.m<sup>-2</sup>). The daily data in resolution 15x15 arc-seconds were extracted from the Meteorological Archival and Retrieval System (MARS) of ECMWF, see ECMWF (2015). For details, see Horálek et al. (2007). The data have been imported into ArcGIS as a point shapefile. Each point represents the centre of a grid cell. The shapefile has been converted into ETRS89-LAEA5210 projection, converted into a 100x100 m resolution raster grid and spatially aggregated into the reference EEA 1x1 km grid.

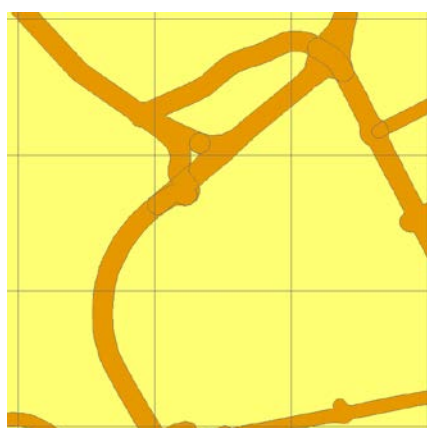
### Population density

Population density (in inhabitants.km<sup>-2</sup>, census 2011) is based on Geostat 2011 grid dataset (Eurostat, 2014). The dataset is in 1x1 km resolution, in the EEA reference grid. For regions not included in the Geostat 2011 dataset we use as alternative sources JRC (2009) and ORNL (2008) data. For details, see Horálek et al. (2017a).

### Road type vector data

GRIP (Meijer et al., 2016) vector road type data base provided by PBL is used. In this data base, road types are distributed into five classes, from highways to local roads and streets. In agreement with the conclusion of Horálek et al. (2017b), classes 1 (Highways, coded T1), 2 (Primary roads, T2) and 3 (Secondary roads, T3) are used. Based on the GRIP vector data, *percentage of the area influenced by traffic* represented by buffers around the roads were calculated in ESRI ArcGIS for individual road type classes 1 – 3 and for their combination (i.e. for classes 1 – 3 together), at all 1x1 km<sup>2</sup> grid cells. A buffer of 75 metres distance at each side from each road vector is taken for the roads of classes 1 (coded T1\_buffer75m) and 2 (T2\_buffer75m), while a buffer of 50 metres is taken for the roads of class 3 (T3\_buffer50m). For motivation, see Horálek et al. (2017b). Figure 3.3 illustrates the buffer around the roads of classes 1 – 3 together (coded T123\_buffer).

**Figure 3.1** Buffer around roads of classes 1 – 3 together, example





# 4 Analysis applying satellite data and QUARK kernel method

## 4.1 Satellite data inclusion in mapping

In this section, we examined potential improvement of the NO<sub>2</sub> mapping by including satellite data in the set of supplementary variables. Satellite data from OMI (see Section 3.3) was used.

For all individual map layers, i.e. rural background, urban background, urban traffic, we compared the mapping variants without and with the inclusion of satellite data. The analysis is based on 2014 data, being the most recent year with all data needed available when this study started.

As the basic variant, we used the current methodology (Horálek et al., 2017c), labelled as (CE)<sup>3</sup>. This variant we compared with a variant labelled as (CEs), consisting of the same set of supplementary variables but with satellite data in addition. Next to this, we examined another four additional variants, by an update (i.e. 2014 data) selection of the supplementary data through a stepwise regression and backwards elimination (Section 2.2). The set of the supplementary variables has been selected in two by two variants, i.e. a variant containing the land cover parameters among the set of supplementary data (AE) and not containing the land cover parameters (NE) – both without (coded (AE) resp. (NE)) and with satellite data included (coded (AEs) resp. (NEs)). Be it noted that for two area types, the same sets of variables (AE) and (AEs) were selected as already used under (CE) and (CEs). For details, see below.

The main motivation for examination of alternative (AE) and (AEs) variants is to deeply explore whether the inclusion of the satellite data improves the NO<sub>2</sub> mapping. If we compared only (CE) and (CEs), one could object that another selection of CLC data (i.e. the most optimal (AE) variant) would also improve the fit, without the use of the satellite data. The additional benefit is the increase of the methodology robustness: The selection of the supplementary data should be robust across the years.

The reason for the examination of variants without land cover parameters (NE) and (NEs) is to explore whether the inclusion of the satellite data improves the fit when the land cover data is not used. Still, in some areas CLC2006 data is not available (see Section 3.4) and a map for these areas might be needed.

The set of supplementary parameter data tested on suitability for inclusion in the linear regression model includes 27 variables. Note that all are in 1x1 km<sup>2</sup> default mapping resolution. The set consists of:

- EMEP model
- altitude:
  - 1x1 km grid altitude
  - floating average of circle radius 5 km around 1x1 km<sup>2</sup> grid cell
- meteorological parameters:
  - wind speed
  - temperature
  - surface net solar radiation
  - relative humidity
- population density

---

<sup>3</sup> Slight differences between the map (and its uncertainty results) presented in Horálek et al. (2017c) and the variant (CE) presented here are caused by the use the most actual CLC2006 version 18 in this paper, while in Horálek et al. (2017c) the CLC2006 version 17 is used.

- road data (as a ratio of 1x1 km grid influenced by traffic represented by buffers around roads):
  - for road type class 1 (coded *T1\_buffer75m*)
  - for road type class 2 (coded *T2\_buffer75m*)
  - for road type class 3 (coded *T3\_buffer50m*)
  - for road type classes 1–3 together (coded *T123\_buffer*)
- land cover type (as percentage of 1x1 km<sup>2</sup> grid and of radius 5 km; see Table 3.1 for further definitions):
  - HDR (coded *HDR\_1km* and *HDR\_5km\_r*)
  - LDR (coded *LDR\_1km* and *LDR\_5km\_r*)
  - IND (coded *IND\_1km* and *IND\_5km\_r*)
  - TRAF (coded *TRAF\_1km* and *TRAF\_5km\_r*)
  - UGR (coded *UGR\_1km* and *UGR\_5km\_r*)
  - AGR (coded *AGR\_1km* and *AGR\_5km\_r*)
  - NAT (coded *NAT\_1km* and *NAT\_5km\_r*)
- satellite data OMI

In the selecting procedure applied on all supplementary data including land cover, exactly the same sets of variables as in use at the current method were selected for rural background and urban traffic areas, both for variants without and with the satellite data. Thus, the variants (AE) and (AEs) were not further examined for these two types of areas, being the same as the variants (CE) and (CEs). By this selection, the robustness of the specific sets of the supplementary data for these two types of areas were confirmed.

For urban background areas, a slightly different set of variables is nominated under (AE) resp. (AEs) compared to the current method (CE) resp. (CEs), for both variants without and with the satellite data. There the set of nominated variables consists of *TRAF\_5km\_r* and *T2\_buffer75m*, instead of *AGR\_1km* and *NAT\_1km* that was used at the current method.

Table 4.1 provides the overview of all the mutually compared variants, including their specific set of nominated supplementary data variables. For the rural background and urban traffic areas four variants were compared, while six variants were compared for the urban background areas. Table 4.2 presents the supplementary variables ultimately nominated and applied, including their relevant statistical performance parameters at both the multiple linear regression and the subsequent interpolation by ordinary kriging of its residuals.

**Table 4.1 List of mutually compared variants of the mapping method**

Lab.	Variant Description	Area type	EMEP	Altitude	Meteo	Pop. dens.	Road data	Land cover	Satel. OMI	
(CE)	Current	Rur. backgr.	+	+	+	+	-	+	-	
		Urb. backgr.	+	+	+	+	+	+	-	
		Urban traffic	+	+	+	-	-	+	-	
(CEs)	Current, including satellite data	Rur. backgr.	+	+	+	+	-	+	+	
		Urb. backgr.	+	+	+	+	+	+	+	
		Urban traffic	+	+	+	-	-	+	+	
(AE)	Alternative	Urb. backgr.	+	+	+	+	+	<sup>(b)</sup>	-	
(AEs)	Alternative, incl. sat.	Urb. backgr.	+	+	+	+	+	+	<sup>(b)</sup>	+
(NE)	No LC data	Rur. backgr.	+	+	+	+	- <sup>(a)</sup>	-	-	
		Urb. backgr.	+	- <sup>(a)</sup>	+	+	+	-	-	
		Urban traffic	+	- <sup>(a)</sup>	- <sup>(a)</sup>	- <sup>(a)</sup>	+	-	-	
(NEs)	No LC data, including satellite data	Rur. backgr.	+	+	+	+	- <sup>(a)</sup>	-	+	
		Urb. backgr.	+	- <sup>(a)</sup>	+	+	+	-	+	
		Urban traffic	+	- <sup>(a)</sup>	- <sup>(a)</sup>	- <sup>(a)</sup>	+	-	+	

<sup>(a)</sup> Not included by the backward stepwise selecting procedure

<sup>(b)</sup> Alternative set of land cover data

**Table 4.2 Parameters of the linear regression models and of the ordinary kriging (nugget, sill, range) of NO<sub>2</sub> annual average for 2014 in rural background, urban background and urban traffic areas for different mapping variants**

linear regr. model + OK of its residuals	(CE) current			(CEs) current + sat.			(AE)	(AEs)	(NE) no LC			(NEs) no LC + sat.		
	rural	urb. b.	urb. tr.	rural	urb. b.	urb. tr.	urb. b.	urb. b.	rural	u. b.	u. tr.	rural	u. b.	u. tr.
	coeff.	coeff.	coeff.	coeff.	coeff.	coeff.	coeff.	coeff.	coeff.	coeff.	coeff.	coeff.	coeff.	coeff.
c (constant)	9.75	17.28	23.37	9.38	16.53	23.12	16.75	15.97	9.29	16.35	22.36	8.70	15.37	20.62
a1 (EMEP model)	0.699	0.550	0.677	0.443	0.318	0.423	0.506	0.271	0.826	0.662	1.031	0.481	0.375	0.744
a2 (altitude_1km)	-0.0085	-0.0082	-0.0215	-0.0093	-0.0089	-0.0219	-0.0090	-0.0096	-0.0090			-0.0100		
a3 (altitude_5km_r)	0.0068	0.0086	0.0216	0.0075	0.0091	0.0216	0.0085	0.0089	0.0047			0.0058		
a4 (wind speed)	-1.135	-1.809	-1.256	-1.308	-2.046	-1.522	-2.062	-2.296	-1.220	-1.456		-1.430	-1.818	
a5 (pop. d. * 1000)	0.624	0.231		0.689	0.252		0.284	0.304	1.039	0.481		1.057	0.501	
a6 (T1_buffer75m)		14.29			14.07		13.23	13.02		19.25			18.71	
a7 (T2_buffer75m)							6.70	7.10		9.87			10.11	
a8 (T123_buffer)											18.43			17.22
a9 (AGR_1km)		-0.0274			-0.0273									
a10 (NAT_1km)		-0.0621			-0.0584									
a11 (LDR_5km_r)	0.0177	0.0127	0.0300	0.0150	0.0107	0.0271	0.0129	0.0108						
a12 (HDR_5km_r)		0.0200	0.0319		0.0217	0.0338	0.0171	0.0188						
a13 (NAT_5km_r)	-0.0040			-0.0039										
a14 (TRAF_5km_r)							0.0304	0.0295						
a15 (satellite OMI)				0.747	0.948	1.013		0.971				0.959	1.120	1.128
<b>adjusted R<sup>2</sup></b>	<b>0.67</b>	<b>0.51</b>	<b>0.38</b>	<b>0.68</b>	<b>0.54</b>	<b>0.39</b>	<b>0.52</b>	<b>0.55</b>	<b>0.61</b>	<b>0.44</b>	<b>0.25</b>	<b>0.64</b>	<b>0.48</b>	<b>0.27</b>
<b>st. err. [µg.m<sup>-3</sup>]</b>	<b>3.37</b>	<b>5.31</b>	<b>10.28</b>	<b>3.29</b>	<b>5.18</b>	<b>10.20</b>	<b>5.26</b>	<b>5.12</b>	<b>3.63</b>	<b>5.69</b>	<b>11.29</b>	<b>3.51</b>	<b>5.51</b>	<b>11.18</b>
nugget	12	16	59	12	15	60	16	15	14	17	78	13	17	77
sill	12	24	133	12	22	132	24	22	14	28	143	13	26	143
range [km]	190	280	570	190	280	570	280	300	190	300	300	560	300	300

Note: Dark grey indicates variables not considered in the variant of the linear regression model. Light grey indicates variables not selected in the variant by the selecting procedure.

## Comparison by cross-validation

The mapping results of all variants are mutually compared by means of the ‘leave one out’ cross-validation (Section 2.3). The comparison results are presented in Table 4.3. The table highlights the statistics of each combination of variant and type of area and provides the level of performance by including a colour ranking: the darker the green marking, the better performance. Lower RMSE and RRMSE and higher  $R^2$  generally indicate better performance; bias closer to zero is also an indication of better performance. Furthermore, the slope  $a$  of the regression equation  $y = ax + b$  should be as close to 1 as possible and the intercept  $b$  as close to zero as possible.

**Table 4.3 Comparison of different mapping variants of spatial interpolation showing RMSE, RRMSE, bias,  $R^2$  and linear regression from the cross-validation scatter plots of  $\text{NO}_2$  annual mean predicted values, 2014. Units:  $\mu\text{g.m}^{-3}$  except RRMSE and  $R^2$ .**

spatial interpolation variant + supplementary data used		rural background areas				
		RMSE	RRMSE	bias	$R^2$	regr. eq.
(CE)	current (EMEP, alt., wind speed, pop. d., LC)	3.3	36.6%	0.0	0.676	$y = 0.694x + 2.8$
(CEs)	current + sat. (EMEP, alt., wind speed, pop. d., LC, sat.)	3.2	35.7%	0.0	0.691	$y = 0.688x + 2.9$
(NE)	no LC (EMEP, alt., wind speed, pop. d.)	3.6	40.0%	0.1	0.613	$y = 0.649x + 3.3$
(NEs)	no LC + sat. (EMEP, alt., wind speed, pop. d., sat.)	3.4	38.0%	0.0	0.650	$y = 0.637x + 3.3$
spatial interpolation variant + supplementary data used		urban background areas				
		RMSE	RRMSE	bias	$R^2$	regr. eq.
(CE)	current (EMEP, alt., w. sp., pop. d., road, LC)	4.8	23.7%	0.0	0.605	$y = 0.639x + 7.3$
(CEs)	current + sat. (EMEP, alt., w. sp., pop. d., road, LC, sat.)	4.7	23.5%	0.0	0.612	$y = 0.636x + 7.3$
(AE)	alternative (EMEP, alt., w. sp., pop. d., road, LC)	4.7	23.3%	0.0	0.620	$y = 0.650x + 7.1$
(AEs)	alternat. + sat. (EMEP, alt., w. sp., pop. d., road, LC, sat.)	4.6	23.0%	0.0	0.627	$y = 0.647x + 7.1$
(NE)	no LC (EMEP, wind speed, pop. d.)	5.2	25.6%	0.0	0.541	$y = 0.586x + 8.4$
(NEs)	no LC + sat. (EMEP, alt., wind speed, pop. d., sat.)	5.1	25.2%	0.0	0.552	$y = 0.584x + 8.4$
spatial interpolation variant + supplementary data used		urban traffic areas				
		RMSE	RRMSE	bias	$R^2$	regr. eq.
(CE)	current (EMEP, alt., wind speed, LC)	8.9	25.4%	0.0	0.533	$y = 0.547x + 15.9$
(CEs)	current + sat. (EMEP, alt., wind speed, LC, sat.)	8.9	25.4%	0.0	0.532	$y = 0.538x + 16.2$
(NE)	no LC (EMEP, road data)	9.9	28.1%	0.1	0.431	$y = 0.457x + 19.2$
(NEs)	no LC + sat. (EMEP, road data, sat.)	9.8	28.0%	0.1	0.434	$y = 0.452x + 19.3$

Not surprisingly, for all types of areas the variants not containing the land cover parameters show poorer results compared to the variants containing land cover, which is in agreement with Horálek et al. (2017b) and confirms the relevance of the inclusion of land cover in the mapping methodology.

It can be seen that for rural background and urban background areas, variants including the satellite data give slightly better results compared to the relevant variant without the satellite data. One can conclude that from the lower RMSE and RRMSE and higher  $R^2$  in the variant (CEs) compared to (CE), and variant (NEs) compared to (NE), and variant (AEs) compared to (AE).

In the urban traffic areas, for the variant without the use of the land cover data the inclusion of satellite data bring a slight improvement in terms of RMSE, RRMSE and  $R^2$ , i.e. (NEs) performs better compared to (NE). However, for the current method the inclusion of satellite data bring no improvement, i.e. (CEs) performs slightly worse compared to (CE).

In the urban background areas, the alternative variants (AE) and (AEs) give slightly better results compared to the current variants (CE) and (CEs). In order to have a robust set of the supplementary variables across the years, it is desirable to compare the current and alternative variants for more years.

## **Conclusion**

*One can conclude that the inclusion of the satellite data provides improvement on the NO<sub>2</sub> mapping methodology in the rural background and urban background areas. Therefore, it is recommended to implement the satellite data in the routine methodology for the rural background and urban background areas. Furthermore, the application of land cover is confirmed firmly to contribute to better performance at all types of area.*

Next to this, it is recommended to consider in the routine mapping the alternate set of the supplementary variables (AEs) in the urban background areas, in dependence to the analysis results in the actual year.

## **4.2 Use of QUARK kernel based model output in mapping**

In this section, we examine the use of QUARK kernel based model output in the ETC/ACM mapping. For doing this, we examine and mutually compare the use of the ‘CHIMERE-SHERPA’ model output (original resolution 7x7 km<sup>2</sup>) and the ‘CHIMERE-SHERPA with QUARK applied’ model output (original grid resolution 125 x 125 m<sup>2</sup>, aggregated into the default mapping resolution of 1x1 km<sup>2</sup>). Although the CHIMERE-SHERPA model outputs are not suitable for the routine use in the ETC/ACM mapping due to their limited domain, with Iceland and large parts of Scandinavia missing, their mutually comparison can show the strength of the QUARK kernel approach, which could be in principle applied on other model output as well (e.g. EMEP). Additionally, we compare these model outputs and their use in the mapping with the EMEP model output (original resolution 50x50 km). This comparison can give us a rough insight on the influence of the model grid resolution. The analysis is based on 2010 data, due to the availability of the QUARK kernel based model data for this year. For the description of the models used, see Section 3.2.

In Section 4.2.1, we mutually compare the model outputs. In Section 4.2.2, we compare their use in mapping. For simplicity, we further code the models as EMEP, CHIMERE and CHIMERE+QUARK.

### **4.2.1 Comparison of modelling data with measurements**

Table 4.4 presents the comparison of different modelling data with station measurements for 2010 data, separately for the rural background, urban background and urban traffic areas. This simple comparison is performed using statistical indicators bias, RMSE and RRMSE, and also R<sup>2</sup> and the regression equation from the scatter plot between the modelled data and the observed concentrations at the measurement stations (Section 2.3). Next to the EMEP (original resolution circa 50x50 km<sup>2</sup>), CHIMERE (original resolution circa 7x7 km<sup>2</sup>) and CHIMERE+QUARK (original grid resolution 125 x 125 m<sup>2</sup> aggregated into 1x1 km<sup>2</sup>) model outputs, we present also the original CHIMERE+QUARK in the 125x125 m<sup>2</sup> resolution. The reason is to show the comparison between the original CHIMERE+QUARK data and the aggregated 1x1 km<sup>2</sup> form of it.

**Table 4.4 Comparison of model outputs against measurement values showing RMSE, RRMSE, bias, R<sup>2</sup> and linear regression from the scatter plots, NO<sub>2</sub> annual mean 2010. Units: µg.m<sup>-3</sup> except RRMSE and R<sup>2</sup>.**

model output		rural background areas				
		RMSE	RRMSE	bias	R <sup>2</sup>	regr. eq.
(E)	model EMEP, cc. 50x50 km	5.4	47.1%	-3.3	0.520	y = 0.569x + 1.7
(C)	model CHIMERE (as used in SHERPA tool), cc. 7x7 km	4.8	41.8%	-0.8	0.542	y = 0.805x + 1.4
(Q)	model CHIMERE + QUARK, aggregated into 1x1 km	4.6	40.3%	-0.8	0.589	y = 0.867x + 0.7
(Q - o)	model CHIMERE + QUARK, original 125x125 m	4.8	41.4%	-0.8	0.569	y = 0.853x + 0.9
model output		urban background areas				
		RMSE	RRMSE	bias	R <sup>2</sup>	regr. eq.
(E)	model EMEP, cc. 50x50 km	16.3	67.4%	-14.5	0.251	y = 0.387x + 0.4
(C)	model CHIMERE (as used in SHERPA tool), cc. 7x7 km	10.9	44.9%	-4.0	0.466	y = 1.137x - 7.4
(Q)	model CHIMERE + QUARK, aggregated into 1x1 km	10.2	41.9%	-2.1	0.470	y = 1.127x - 5.2
(Q - o)	model CHIMERE + QUARK, original 125x125 m	10.1	41.7%	-2.5	0.487	y = 1.148x - 6.1
model output		urban traffic areas				
		RMSE	RRMSE	bias	R <sup>2</sup>	regr. eq.
(E)	model EMEP, cc. 50x50 km	33.1	82.7%	-30.4	0.168	y = 0.178x + 2.6
(C)	model CHIMERE (as used in SHERPA tool), cc. 7x7 km	22.0	54.9%	-15.6	0.231	y = 0.514x + 2.4
(Q)	model CHIMERE + QUARK, aggregated into 1x1 km	20.2	50.5%	-12.8	0.226	y = 0.509x + 5.2
(Q - o)	model CHIMERE + QUARK, original 125x125 m	19.7	49.2%	-10.9	0.243	y = 0.584x + 4.6

To guarantee the comparability between the different models, a common domain has been considered in the scatter plot comparison, namely the smaller model domain of the CHIMERE and CHIMERE+QUARK models. This secures that only the data from measurement stations, which are covered by all the models are taken into account.

A direct comparison of different model outputs against measurement data for 2010 shows better agreement of both CHIMERE and CHIMERE+QUARK compared to EMEP, for all three area types, with the most prominent difference in the urban background areas. The reason is probably related to the higher resolution of both CHIMERE and the two CHIMERE+QUARK model outputs compared to the EMEP model output.

Comparing the CHIMERE with both resolutions of CHIMERE+QUARK, one can see somewhat better agreement of the CHIMERE+QUARK with the measurements compared to the pure CHIMERE in the urban background and urban traffic areas. The CHIMERE+QUARK in 125x125 m resolution gives better results compared to CHIMERE+QUARK in 1x1 km for urban traffic areas, but not for the background areas, neither rural nor urban background. This is in line with the fact that the QUARK kernel method adds a traffic contribution on top of background concentrations (Section 3.2). Next to this, it should be noted that the CHIMERE+QUARK shows only slightly better agreement with the measurement compared to the pure CHIMERE in terms of bias; both model outputs are underestimated. This can be explained by uncertainties in emission inventories (especially road traffic emissions) and by the fact that for NO<sub>2</sub> which behaves as a local pollutant, concentrations are quite difficult to predict with chemistry-transport models' resolution (even with QUARK-like corrections). Since there is no use of data assimilation or data fusion with the measurements in the experiments conducted with CHIMERE nor CHIMERE+QUARK and presented in this report, underestimation of concentration maps is not corrected.

#### 4.2.2 Inclusion of 'CHIMERE with QUARK applied' model output in mapping

For all individual map layers, i.e. rural background, urban background, urban traffic, we compared the mapping variants using EMEP, CHIMERE and CHIMERE+QUARK model outputs. Be it noted that

from now on, the CHIMERE+QUARK aggregated into 1x1 km<sup>2</sup> is used, as described in Section 3.2. The analysis is based on 2010 data as modelling data were readily available.

As the basic variant, we used the current methodology (Horálek et al., 2017c) supplemented with the satellite data in the rural and urban background areas, based on the recommendation of Section 4.1. As default model the EMEP is used in this variant. We label this variant as (CE). This variant was compared with the same variants, but now using CHIMERE resp. CHIMERE+QUARK model outputs instead of the EMEP model output; we label these variants as (CC) and (CQ).

Next to this, we examined several additional variants, by selection of the supplementary data through a stepwise regression and backwards elimination (Section 2.2). The set of the supplementary variables has been selected in two by three variants, i.e. containing and not containing the land cover parameters among the supplementary data – using either EMEP, CHIMERE or CHIMERE+QUARK model outputs. Like in Section 4.1, the reason for the examination of the variants without containing the land cover parameters is that CLC2006 data is not available for the entire mapping area (see Section 3.4) and to cover these areas might be needed. The variants selected on all supplementary data by the backward stepwise procedure are called as ‘alternative’ and labelled as (AE), (AC) and (AQ). The variants not containing land cover are labelled as (NE), (NC) and (NQ).

The set of supplementary parameter data tested on suitability for inclusion in the linear regression model included – apart from the variant model output – the similar set of variables like in Section 3.2. Note that all are in 1x1 km<sup>2</sup> default mapping resolution. The set consists of:

- EMEP or CHIMERE or CHIMERE+QUARK model output
- altitude:
  - 1x1 km grid altitude
  - floating average of circle radius 5 km around 1x1 km<sup>2</sup> grid cell
- meteorological parameters:
  - wind speed
  - temperature
  - surface net solar radiation
  - relative humidity
- population density
- road data (as ratio of 1x1 km grid influenced by traffic represented by buffers around roads):
  - for road type class 1 (coded *T1\_buffer75m*)
  - for road type class 2 (coded *T2\_buffer75m*)
  - for road type class 3 (coded *T3\_buffer50m*)
  - for road type classes 1–3 together (coded *T123\_buffer*)
- land cover type (as ratio of 1x1 km<sup>2</sup> grid and of radius 5 km):
  - HDR (coded *HDR\_1km* and *HDR\_5km\_r*)
  - LDR (coded *LDR\_1km* and *LDR\_5km\_r*)
  - IND (coded *IND\_1km* and *IND\_5km\_r*)
  - TRAF (coded *TRAF\_1km* and *TRAF\_5km\_r*)
  - UGR (coded *UGR\_1km* and *UGR\_5km\_r*)
  - AGR (coded *AGR\_1km* and *AGR\_5km\_r*)
  - NAT (coded *NAT\_1km* and *NAT\_5km\_r*)
- satellite data OMI

In the selecting procedure applied on all supplementary data sources including land cover, exactly the same set of variables as in use at the current method were nominated for rural background areas. Thus, the alternative variants (AE), (AC) and (AQ) were not further examined for this type of areas, being the same as the variants (CE), (CC) and (CQ). A slightly different set of variables is nominated for urban background and urban traffic areas. As a result, for the rural background six variants were selected for comparison on their performance, while nine variants were for selected for the urban background and urban traffic areas. For the overview of all the mutually compared method variants, see Table 4.5.

**Table 4.5 List of mutually compared variants of the mapping method**

Lab.	Variant Description	Area type	EM.	CH.	CH.+Q.	Altitude	Meteo	Pop. dens.	Road data	Land cover	Sat. OMI
(CE)	Current, EMEP	Rur. backgr.	+	-	-	+	+	+	-	+	+
		Urb. backgr.	+	-	-	+	+	+	+	+	+
		Urban traffic	+	-	-	+	+	-	-	+	-
(CC)	Current, CHIMERE	Rur. backgr.	-	+	-	+	+	+	-	+	+
		Urb. backgr.	-	+	-	+	+	+	+	+	+
		Urban traffic	-	+	-	+	+	-	-	+	-
(CQ)	Current, CHIMERE +QUARK	Rur. backgr.	-	-	+	+	+	+	-	+	+
		Urb. backgr.	-	-	+	+	+	+	+	+	+
		Urban traffic	-	-	+	+	+	-	-	+	-
(AE)	Alternative, EMEP	Urb. backgr.	+	-	-	+	+	+	+	+( <sup>b</sup> )	+
		Urban traffic	+	-	-	- ( <sup>a</sup> )	+	- ( <sup>a</sup> )	- ( <sup>a</sup> )	+( <sup>b</sup> )	+
(AC)	Alternative, CHIMERE	Urb. backgr.	-	+	-	+	+	+	+	+( <sup>b</sup> )	+
		Urban traffic	-	+	-	- ( <sup>a</sup> )	+	- ( <sup>a</sup> )	- ( <sup>a</sup> )	+( <sup>b</sup> )	+
(AQ)	Alternative, CHIM.+Q.	Urb. backgr.	-	-	+	+	+	+	+	+( <sup>b</sup> )	+
		Urban traffic	-	-	+	- ( <sup>a</sup> )	+	- ( <sup>a</sup> )	- ( <sup>a</sup> )	+( <sup>b</sup> )	+
(NE)	No LC data, EMEP	Rur. backgr.	+	-	-	+	+	+	+	-	+
		Urb. backgr.	+	-	-	- ( <sup>a</sup> )	+	+	+	-	+
		Urban traffic	+	-	-	- ( <sup>a</sup> )	- ( <sup>a</sup> )	+	+	-	+
(NC)	No LC data, CHIMERE	Rur. backgr.	-	+	-	+	+	+	+	-	+
		Urb. backgr.	-	+	-	- ( <sup>a</sup> )	+	+	+	-	+
		Urban traffic	-	+	-	- ( <sup>a</sup> )	- ( <sup>a</sup> )	+	+	-	+
(NQ)	No LC data, CHIMERE +QUARK	Rur. backgr.	-	-	+	+	+	+	+	-	+
		Urb. backgr.	-	-	+	- ( <sup>a</sup> )	+	+	+	-	+
		Urban traffic	-	-	+	- ( <sup>a</sup> )	- ( <sup>a</sup> )	+	+	-	+

(<sup>a</sup>) Not included by the backward stepwise selecting procedure

(<sup>b</sup>) Alternative set of land cover data

Wherever possible, we kept at the selection of the supplementary data the set of variables identical for all three models involved at both the ‘alternative’ and ‘no LC data’ variants. However, in some cases one or two variables are flagged as statistically not significant and thus are dropped from the linear regression model.

Table 4.6 presents the supplementary variables ultimately nominated and applied, including their relevant statistical performance parameters at both the multiple linear regression and the subsequent interpolation by ordinary kriging of its residuals.

**Table 4.6 Parameters of the linear regression models and of the ordinary kriging (nugget, sill, range) of NO<sub>2</sub> annual average for 2010 in rural background, urban background and urban traffic areas for different method variants**

linear regr. model + OK of its residuals	(CE) current, EMEP			(CC) curr., CHIMERE			(CQ) curr., CH.+Q.			(AE) alt., EMEP		(AC) alt., CHIM.	
	rural	urb. b.	urb. tr.	rural	urb. b.	urb. tr.	rural	urb. b.	urb. tr.	urb. b.	urb. tr.	urb. b.	urb. tr.
	coeff.	coeff.	coeff.	coeff.	coeff.	coeff.	coeff.	coeff.	coeff.	coeff.	coeff.	coeff.	coeff.
c (constant)	11.53	24.71	31.86	9.23	21.71	30.93	9.53	20.14	31.12	17.10	36.27	22.24	35.41
a1 (EMEP model)	0.466	0.214	0.530							0.227	0.342		
a2 (CHIM. model)				0.251	0.276	0.265						0.502	0.157
a3 (CH.+Q. model)							0.261	0.276	0.260				
a4 (altitude_1km)	-0.0111	-0.0078	-0.0219	-0.0115	-0.0137	-0.0305	-0.0086	-0.0088	-0.0242	-0.0140		-0.0170	
a5 (altitude_5km_r)	0.0086	0.0062	0.0185	0.0093	0.0106	0.0234	0.0064	0.0061	0.0166	0.0153		0.0157	
a6 (wind speed)	-1.591	-3.084	-2.117	-1.240	-1.954	-1.581	-1.284	-1.803	-1.718	-2.960	-2.522	-2.107	-2.065
a7 (s. solar rad.)										0.644		<i>n. sign.</i>	
a8 (pop. d. * 1000)	1.854	0.200		1.793	0.109		1.474	0.145					
a9 (T1_buffer75m)		13.103						<i>n. sign.</i>		12.01		9.88	
a10 (T2_buffer75m)										7.90		7.08	
a11 (T123_buffer)													
a12 (AGR_1km)		-0.0462			-0.0572			-0.0466		-0.0547		-0.0526	
a13 (HDR_1km)										0.0658		0.0434	
a14 (NAT_1km)		-0.0511			-0.0531			-0.0457					
a15 (AGR_5km_r)											-0.0064		-0.0078
a16 (LDR_5km_r)	0.0136	0.0106	0.0319	0.0067	0.0050	0.0298	0.0075	0.0062	0.0303	0.0110	0.0238	0.0041	0.0206
a17 (HDR_5km_r)		0.0214	0.0363			0.0185		<i>n. sign.</i>	0.0213		0.0305		0.0184
a18 (NAT_5km_r)	-0.0036			-0.0026			-0.0028			-0.0098		-0.0070	
a19 (satellite OMI)	0.760	1.045		1.261	0.627		1.247	0.752		1.281	0.809	0.766	1.023
<b>adjusted R<sup>2</sup></b>	<b>0.74</b>	<b>0.51</b>	<b>0.32</b>	<b>0.73</b>	<b>0.56</b>	<b>0.32</b>	<b>0.73</b>	<b>0.55</b>	<b>0.32</b>	<b>0.53</b>	<b>0.33</b>	<b>0.59</b>	<b>0.33</b>
<b>st. err. [µg.m<sup>-3</sup>]</b>	<b>3.18</b>	<b>5.82</b>	<b>12.00</b>	<b>3.24</b>	<b>5.47</b>	<b>11.97</b>	<b>3.23</b>	<b>5.55</b>	<b>11.96</b>	<b>5.67</b>	<b>11.98</b>	<b>5.32</b>	<b>11.93</b>
nugget	9	18	99	9	18	99	8	19	102	16	103	16	103
sill	10	28	154	11	25	151	11	27	150	28	155	25	153
range [km]	710	150	100	700	150	90	680	150	90	150	90	150	90

linear regr. model + OK of its residuals	(AQ) alt., CH+Q		(NE) no LC, EMEP			(NQ) no LC, CHIMERE			(NQ) no LC, CH.+Q.		
	urb. b.	urb. tr.	rural	urb. b.	urb. tr.	rural	urb. b.	urb. tr.	rural	urb. b.	urb. tr.
	coeff.	coeff.	coeff.	coeff.	coeff.	coeff.	coeff.	coeff.	coeff.	coeff.	coeff.
c (constant)	21.16	33.42	11.12	20.20	23.81	8.15	17.65	23.81	8.66	16.47	23.76
a1 (EMEP model)			0.494	0.277	0.692						
a2 (CHIM. model)						0.305	0.278	0.337			
a3 (CH.+Q. model)	0.251	0.176							0.318	0.272	0.327
a4 (altitude_1km)	-0.0133		-0.0109			-0.0115			-0.0084		
a5 (altitude_5km_r)	0.0127		0.0062			0.0079			0.0047		
a6 (wind speed)	-1.948	-1.856	-1.729	-2.502		-1.202	-1.689		-1.260	-1.435	
a7 (s. solar rad.)	<i>n. sign.</i>										
a8 (pop. d. * 1000)			2.11	0.44	0.25	1.74	0.17	<i>n. sign.</i>	1.61	0.22	<i>n. sign.</i>
a9 (T1_buffer75m)	<i>n. sign.</i>		19.47			17.71			<i>n. sign.</i>		
a10 (T2_buffer75m)	4.50										
a11 (T123_buffer)			12.88	19.10		12.11	17.30		7.88	11.67	
a12 (AGR_1km)	-0.0460										
a13 (HDR_1km)	0.0490										
a14 (NAT_1km)											
a15 (AGR_5km_r)		-0.0069									
a16 (LDR_5km_r)	0.0053	0.0211									
a17 (HDR_5km_r)		0.0193									
a18 (NAT_5km_r)	-0.0078										
a19 (satellite OMI)	0.868	1.046	0.897	1.294	0.842	1.263	0.835	1.064	1.233	0.989	1.314
<b>adjusted R<sup>2</sup></b>	<b>0.57</b>	<b>0.33</b>	<b>0.72</b>	<b>0.45</b>	<b>0.23</b>	<b>0.73</b>	<b>0.54</b>	<b>0.27</b>	<b>0.72</b>	<b>0.53</b>	<b>0.26</b>
<b>st. err. [µg.m<sup>-3</sup>]</b>	<b>5.40</b>	<b>11.89</b>	<b>3.31</b>	<b>6.17</b>	<b>12.81</b>	<b>3.25</b>	<b>5.62</b>	<b>12.40</b>	<b>3.29</b>	<b>5.70</b>	<b>12.50</b>
nugget	18	104	10	18	97	8	19	98	9	20	104
sill	26	152	11	32	175	10	27	161	11	29	165
range [km]	150	90	680	130	90	680	150	90	680	170	90

Note: Dark grey indicates variables not considered in the variant of the linear regression model. Light grey indicates variables not selected in the variant by the selecting procedure.

## Comparison by cross-validation

Table 4.7 presents the mapping results of all variants, with their different sets of supplementary data that are mutually compared by means of the ‘leave one out’ cross-validation (Section 2.3), separate for the rural background, urban background and urban traffic areas. The table highlights the statistics of each combination of variant and type of area and provides the level of best performance by including a colour ranking: the darker the green marking, the better performance).

To guarantee comparability between the different variants and models, a common domain has been considered in the scatter plot comparison, namely the smaller modelling domain of the CHIMERE and CHIMERE+QUARK models. This secures that only the data from measurement stations, which are covered by all the models are taken into account.

**Table 4.7 Comparison of different method variants of spatial interpolation showing RMSE, RRMSE, bias, R<sup>2</sup> and linear regression from the cross-validation scatter plots of NO<sub>2</sub> annual mean predicted values, 2010. Units: µg.m<sup>-3</sup> except RRMSE and R<sup>2</sup>.**

spatial interpolation variant + supplementary data used		rural background areas				
		RMSE	RRMSE	bias	R <sup>2</sup>	regr. eq.
(CE)	current, EMEP (EMEP, alt., w. sp, pop. d., LC, sat.)	3.1	26.8%	0.1	0.753	y = 0.773x + 2.7
(CC)	current, CHIMERE (CHIM., alt., w. sp., pop. d., LC, sat.)	3.1	26.8%	0.1	0.754	y = 0.774x + 2.6
(CQ)	curr., CHIM.+QUARK (CH+Q, alt., w.sp., pop.d., LC, sat.)	3.1	26.6%	0.1	0.758	y = 0.779x + 2.6
(NE)	no LC, EMEP (EMEP, alt., w. sp, pop. d., road, sat.)	3.2	27.7%	0.0	0.737	y = 0.761x + 2.8
(NC)	no LC, CHIMERE (CHIM., alt., w. sp, pop. d., road, sat.)	3.1	26.7%	0.1	0.755	y = 0.776x + 2.6
(NQ)	no LC, CHIM.+QUARK (CH+Q, alt., w.sp., pop.d., sat.)	3.1	27.3%	0.1	0.744	y = 0.769x + 2.7
spatial interpolation variant + supplementary data used		urban background areas				
		RMSE	RRMSE	bias	R <sup>2</sup>	regr. eq.
(CE)	current, EMEP (EMEP, alt., w.sp., pop.d., road, LC, sat.)	5.2	21.4%	0.0	0.605	y = 0.636x + 8.8
(CC)	current, CHIM. (CHIM., alt., w.sp., pop.d., road, LC, sat.)	5.0	20.7%	0.0	0.631	y = 0.638x + 8.8
(CQ)	curr., CHIM.+QUARK (CH+Q., alt., w.sp., pop.d., LC, sat.)	5.1	20.9%	0.0	0.622	y = 0.631x + 9.0
(AE)	altern., EMEP (EM., alt., w.sp., s.s.r., pop.d., road, LC, sat.)	5.1	21.1%	0.1	0.619	y = 0.636x + 8.9
(AC)	altern., CHIMERE (CHIM., alt., w.sp., pop.d., road, LC, sat.)	4.9	20.2%	0.0	0.648	y = 0.660x + 8.3
(AQ)	altern., CHIM.+Q. (CH+Q., alt., w.sp., pop.d., road, LC, sat.)	5.0	20.6%	0.0	0.636	y = 0.650x + 8.5
(NE)	no LC, EMEP (EMEP, w. sp., pop. dens., road, sat.)	5.6	22.9%	0.1	0.550	y = 0.576x + 10.4
(NC)	no LC, CHIMERE (CHIM., w. sp., pop. dens., road, sat.)	5.2	21.4%	0.0	0.606	y = 0.611x + 9.5
(NQ)	no LC, CHIM.+QUARK (CH+Q, w. sp., pop. d., road, sat.)	5.3	21.7%	0.0	0.594	y = 0.602x + 9.7
spatial interpolation variant + supplementary data used		urban traffic areas				
		RMSE	RRMSE	bias	R <sup>2</sup>	regr. eq.
(CE)	current, EMEP (EMEP, alt., wind speed, LC)	10.6	26.4%	0.0	0.477	y = 0.499x + 20.0
(CC)	current, CHIMERE (CHIM., alt., wind speed, LC)	10.5	26.3%	0.0	0.482	y = 0.503x + 19.9
(CQ)	current, CHIMERE+QUARK (CH.+Q., alt., wind speed, LC)	10.6	26.4%	0.0	0.484	y = 0.504x + 19.9
(AE)	alternative, EMEP (EMEP, wind speed, LC, sat.)	10.5	26.2%	0.0	0.472	y = 0.501x + 20.0
(AC)	alternative, CHIMERE (CHIM., wind speed, LC, sat.)	10.5	26.1%	0.0	0.476	y = 0.513x + 19.5
(AQ)	alternative, CHIM.+QUARK (CH.+Q., w. speed, LC, sat.)	10.4	26.1%	0.0	0.475	y = 0.514x + 19.5
(NE)	no LC, EMEP (EMEP, pop. dens., road, sat.)	11.2	28.1%	0.1	0.405	y = 0.446x + 22.3
(NC)	no LC, CHIMERE (CHIM., road, sat.)	10.8	27.0%	0.0	0.446	y = 0.470x + 21.2
(NQ)	no LC, CHIMERE+QUARK (CH.+Q., road, sat.)	11.0	27.5%	0.0	0.427	y = 0.457x + 21.7

Like in Section 4.1, for all types of areas the variants not containing the land cover parameters show poorer results compared to the variants containing land cover, which is in agreement with Horálek et al. (2017b) and confirms the relevance of the inclusion of land cover in the mapping methodology.

By comparing the results of the three models applied in the mapping process, i.e. variants using EMEP, CHIMERE and CHIMERE+QUARK, one observes at the rural areas quite similar outcomes with a very small improvement when using the CHIMERE+QUARK data in the case of the current method, and slight improvement when using the pure CHIMERE model in the case of the method with no land cover.

At the urban background and urban traffic areas, slight improvement of variants using CHIMERE and CHIMERE+QUARK models as supplementary data source is observed, compared to variants with the use of EMEP model. Surprisingly, the application of the CHIMERE+QUARK does not improve mapping results, when compared to the variants with the pure CHIMERE model. Even, in the urban background areas, the variants using pure CHIMERE give slightly better results compared to CHIMERE+QUARK. The reason probable is that a large part of the spatial variability has already been captured by the currently used set of supplementary data. It must be noted here however that the aggregation of the QUARK 125x125 m<sup>2</sup> model output to 1x1 km largely flattens out the road-side gradients introduced by the kernel methodology.

In the urban background and urban traffic areas, the alternative variants (AE), (AC) and (AQ) give slightly better results compared to the current variants (CE), (CC) and (CQ).

### **Comparison of point measurement values with the predicted grid value**

Next to the above presented cross-validation, a simple comparison was made between the point observation values and interpolated predicted 1x1 km grid values, for variants (CE), (CC) and (CQ). This point-grid comparison indicates to what extent the predicted value of a grid cell represents the corresponding measurement values at stations located in that cell.

The comparison has been made primarily for the separate rural, separate urban background and separate urban traffic map layers at 1x1 km resolution. Besides, the comparison has been done also for the merged background layer and the final merged map. Table 4.8 presents the results of this comparison.

One can see that the final combined map in 1x1 km resolution is representative for rural and urban background areas, but not for urban traffic areas.

By comparing the results of the three models applied in the mapping process, i.e. variants (CE), (CC) and (CQ), one can see slightly better results for variants using CHIMERE and CHIMERE+QUARK, i.e. (CC) and (CQ), compared to the variant using EMEP, i.e. (CE). The variants (CC) and (CQ) give similar results.

**Table 4.8 Statistical indicators from the scatter plots for the predicted grid values from separate (rural, urban background or urban traffic) map layers and final combined map versus the measurement point values for rural, urban background and urban traffic stations for NO<sub>2</sub> annual average 2010**

		rural background stations				
		RMSE	RRMSE	bias	R <sup>2</sup>	lin. r. equation
(CE)	grid prediction, 1x1 km rural background map layer	2.9	25.2%	0.1	0.781	y = 0.786x + 2.54
	grid prediction, 1x1 km merged background map layer	3.5	30.6%	0.6	0.708	y = 0.826x + 2.57
	grid prediction, 1x1 km final merged map	3.6	31.4%	0.7	0.700	y = 0.836x + 2.54
(CC)	grid prediction, 1x1 km rural background map layer	2.8	24.3%	0.0	0.796	y = 0.794x + 2.42
	grid prediction, 1x1 km merged background map layer	3.1	27.0%	0.4	0.757	y = 0.802x + 2.70
	grid prediction, 1x1 km final merged map	3.2	27.7%	0.5	0.747	y = 0.811x + 2.66
(CQ)	grid prediction, 1x1 km rural background map layer	2.8	24.0%	0.0	0.802	y = 0.799x + 2.35
	grid prediction, 1x1 km merged background map layer	3.1	26.7%	0.5	0.765	y = 0.816x + 2.59
	grid prediction, 1x1 km final merged map	3.2	27.5%	0.6	0.755	y = 0.825x + 2.56
		urban/suburban background stations				
		RMSE	RRMSE	bias	R <sup>2</sup>	lin r. equation
(CE)	grid prediction, 1x1 km urban background map layer	3.9	16.1%	0.0	0.778	y = 0.730x + 6.55
	grid prediction, 1x1 km merged background map layer	4.5	18.7%	-0.3	0.700	y = 0.724x + 6.37
	grid prediction, 1x1 km final merged map	4.9	20.3%	1.0	0.670	y = 0.756x + 6.92
(CC)	grid prediction, 1x1 km urban background map layer	4.0	16.6%	0.0	0.767	y = 0.713x + 6.99
	grid prediction, 1x1 km merged background map layer	4.5	18.5%	-0.4	0.707	y = 0.721x + 6.41
	grid prediction, 1x1 km final merged map	4.8	19.9%	1.0	0.680	y = 0.759x + 6.84
(CQ)	grid prediction, 1x1 km urban background map layer	4.1	16.8%	0.0	0.761	y = 0.707x + 7.12
	grid prediction, 1x1 km merged background map layer	4.5	18.6%	-0.3	0.703	y = 0.715x + 6.60
	grid prediction, 1x1 km final merged map	4.9	20.2%	1.0	0.674	y = 0.753x + 7.00
		urban/suburban traffic stations				
		RMSE	RRMSE	bias	R <sup>2</sup>	lin. r. equation
(CE)	grid prediction, 1x1 km urban traffic map layer	7.8	19.4%	0.0	0.723	y = 0.636x + 14.57
	grid prediction, 1x1 km final merged map	17.0	42.4%	-12.3	0.355	y = 0.340x + 14.11
(CC)	grid prediction, 1x1 km urban traffic map layer	7.7	19.3%	0.0	0.724	y = 0.647x + 14.16
	grid prediction, 1x1 km final merged map	17.0	42.5%	-12.5	0.371	y = 0.342x + 13.86
(CQ)	grid prediction, 1x1 km urban traffic map layer	7.9	19.6%	0.0	0.714	y = 0.642x + 14.37
	grid prediction, 1x1 km final merged map	16.9	42.1%	-12.3	0.375	y = 0.342x + 14.03

## Conclusion

From the above, one can conclude that the application of the QUARK kernel method on the model used in the mapping does not necessarily lead to an improvement of mapping results at the presently used 1x1 km<sup>2</sup> resolution.

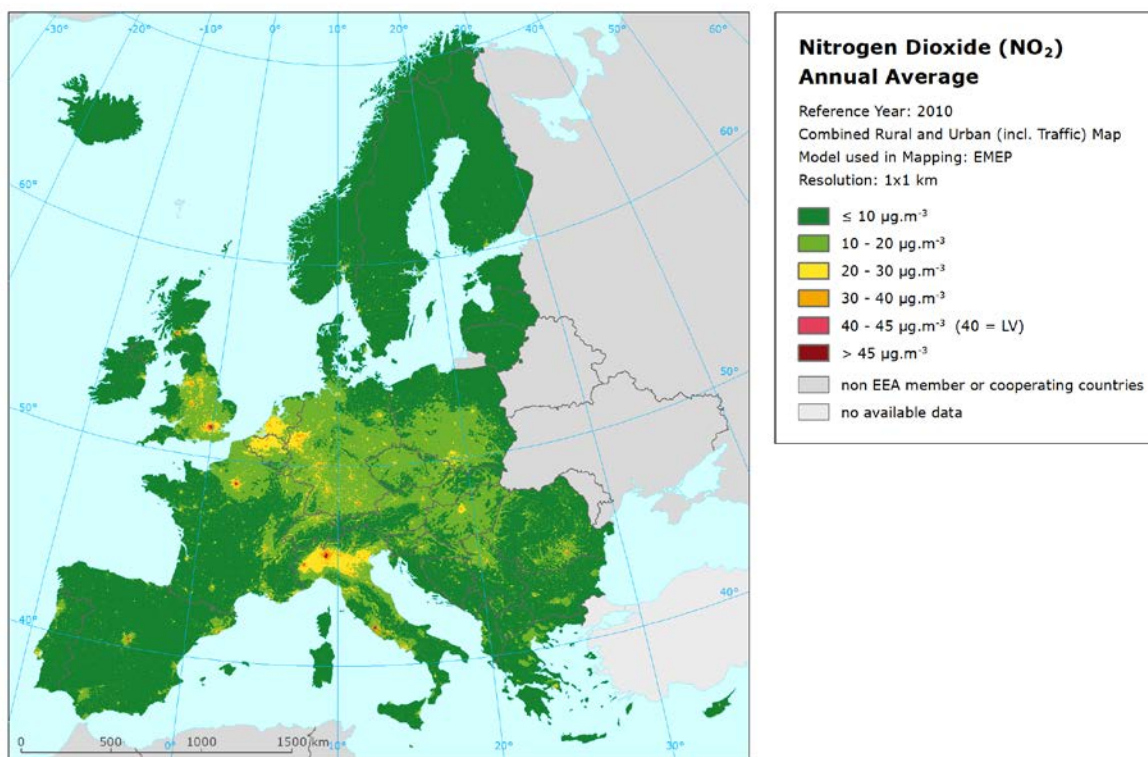
Next to this, it can be recommended to consider in the routine mapping the alternate set of the supplementary variables in the urban background and urban traffic areas, in dependence to the analysis results in the actual year.

## Mapping results

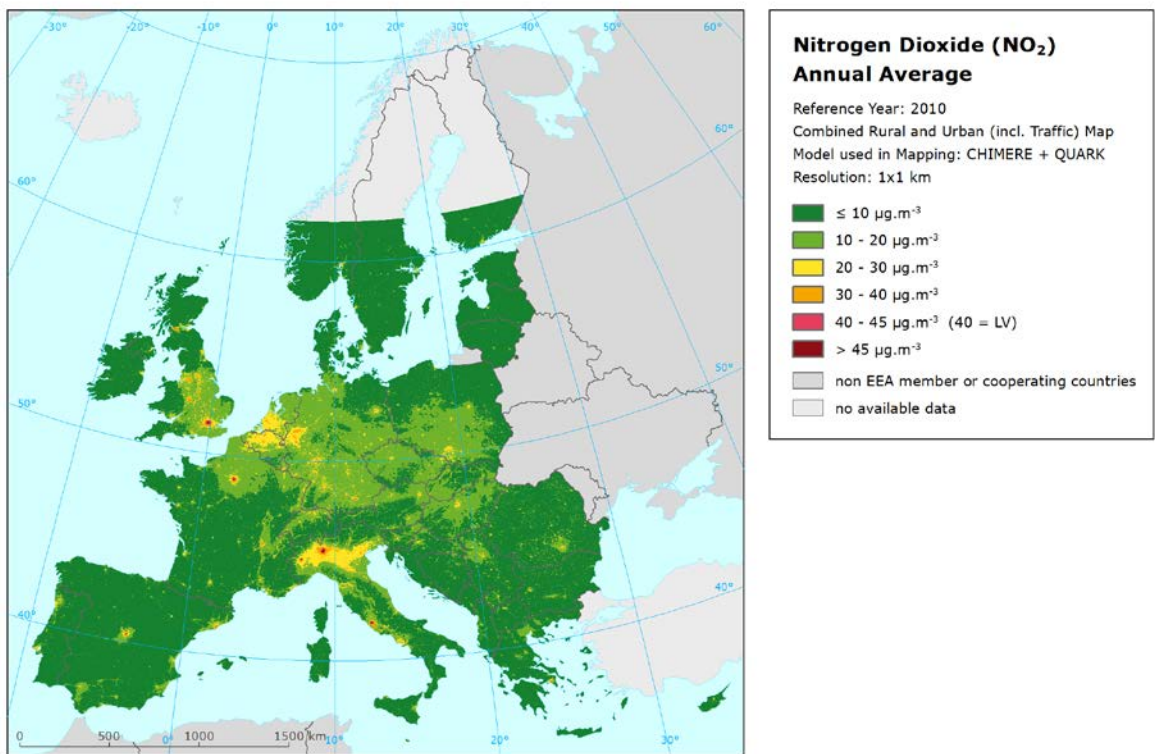
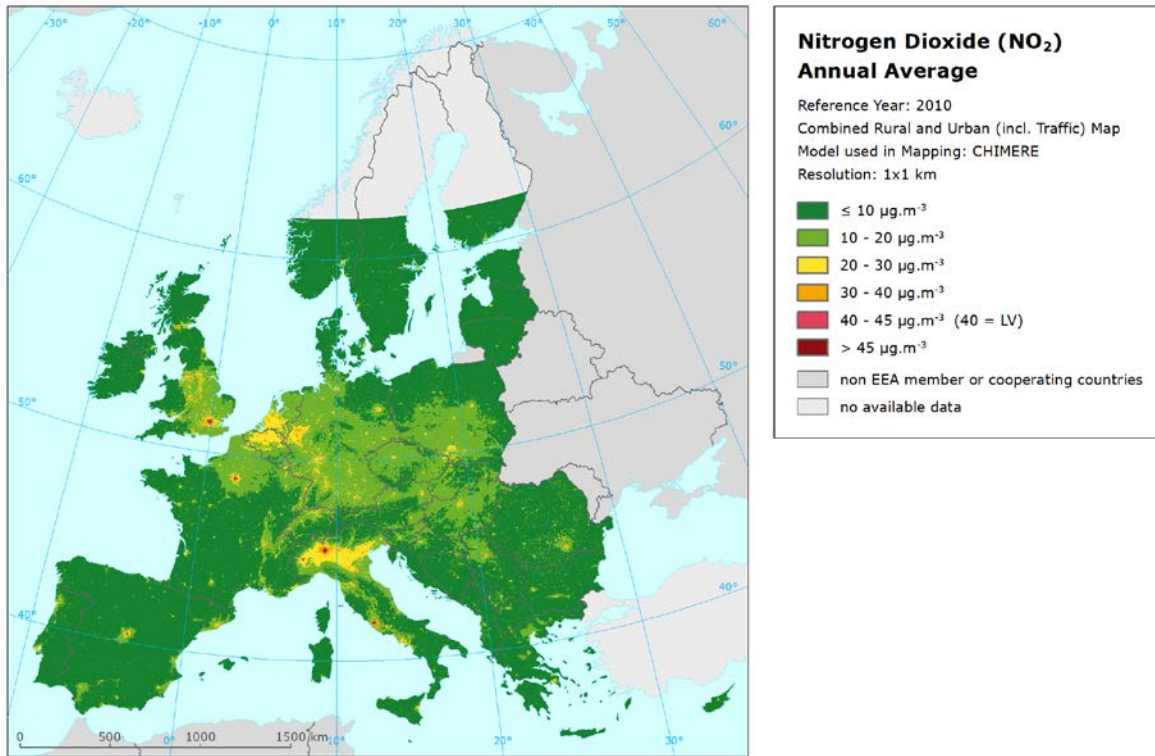
Map 4.1 presents the combined final map as a result of the merging of the rural background, urban background and urban traffic map layers created by means of the current methodology using EMEP model, i.e. variant (CE).

Map 4.2 gives the same map created by means of the current method, but using CHIMERE (top) and CHIMERE+QUARK (bottom) models instead of EMEP, i.e. variants (CC) and (CQ).

**Map 4.1 Concentration map of NO<sub>2</sub> annual average using EMEP model, 2010**

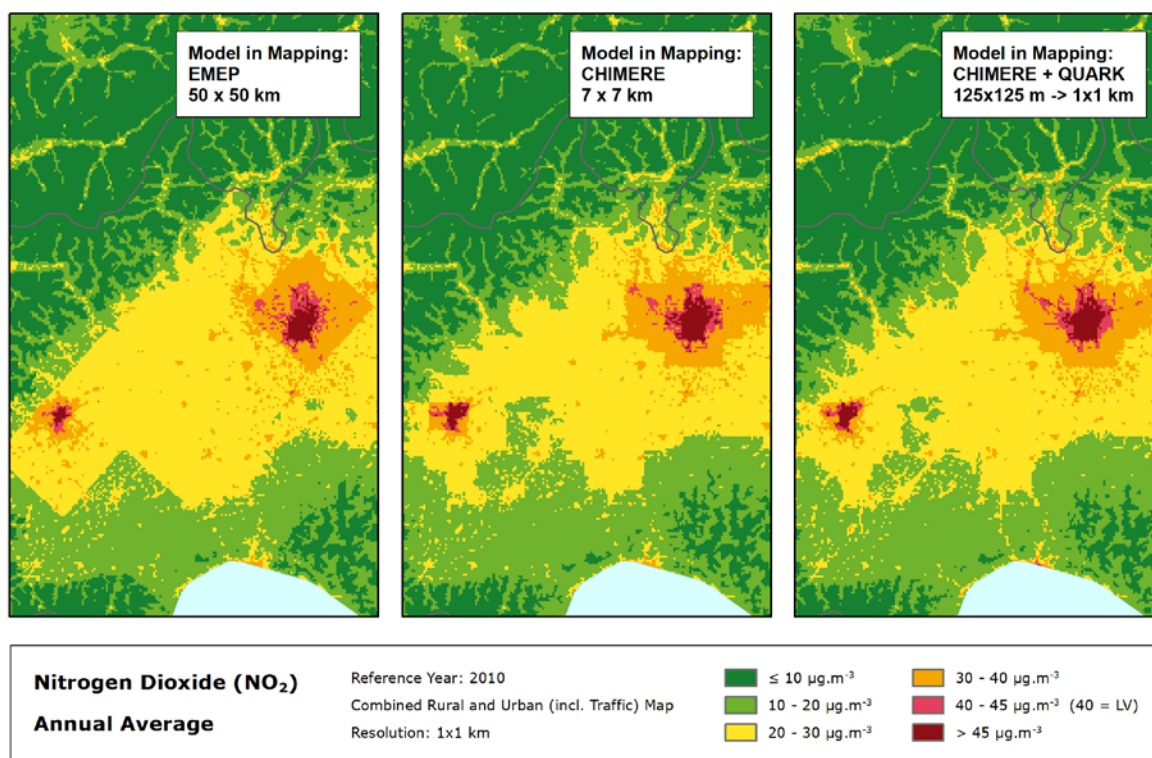


**Map 4.2 Concentration map of NO<sub>2</sub> annual average using CHIMERE (top) and CHIMERE+QUARK (bottom) models, 2010**



Map 4.3 shows an extract of the NO<sub>2</sub> concentration maps covering the western Po valley using three different models EMEP (left), CHIMERE (middle) and CHIMERE+QUARK (right) in mapping, i.e. variants (CE), (CC) and (CQ). In the maps, one can see the elevated NO<sub>2</sub> concentrations in large cities of Milan and Turin. In the variant using EMEP, the underlying 50x50 km<sup>2</sup> grid is clearly visible. Similarly, although less notably, the underlying 7x7 km<sup>2</sup> grid can be seen in the variant using CHIMERE.

**Map 4.3** Concentration map of NO<sub>2</sub> annual average using EMEP (left), CHIMERE (middle) and CHIMERE+QUARK (right) models, 2010, western Po valley





## 5 Conclusion

The paper examines the potential improvement of the ETC/ACM “regression – interpolation – merging” mapping of NO<sub>2</sub> using satellite data and model output with the QUARK kernel downscaling method applied. At first, the inclusion of the OMI satellite data has been tested. Next to this, the mapping variant using ‘CHIMERE-SHERPA with QUARK kernel applied’ model output has been examined and compared with the mapping variants using ‘CHIMERE-SHERPA’ and ‘EMEP’ model outputs.

Additionally, Annex 2 discusses potential alternative coupling of the QUARK kernel method with the ETC/ACM mapping methodology. This method is not directly in line with the current mapping methodology, however it would allow for traffic scenario calculations. Next to this, Annex 2 discussed a potential refinement of the resolution in the map construction and suggests several approaches for such a refinement.

### **Satellite data inclusion**

One can conclude that the inclusion of the satellite data provides improvement on the NO<sub>2</sub> mapping methodology in the rural and urban background areas. Therefore, it is recommended to implement the satellite data in the routine methodology for the rural and urban background areas. This recommendation applies to OMI based satellite data product OMNO2d level 3, which is being produced by NASA at the regular basis, safely in advance of the time when the routine maps are to be constructed. The OMNO2d satellite data is available in 0.25°x0.25° (circa 20x20 km) resolution. When the TROPOMI satellite NO<sub>2</sub> data is routinely produced, it will be a candidate for the use in routine mapping, due to its increased resolution of 7x7 km<sup>2</sup>.

### **‘QUARK kernel method’ based model output use in mapping**

The use of the QUARK kernel based downscaling method model output in the ETC/ACM mapping have been examined. For doing this, we have compared the use of the ‘CHIMERE-SHERPA’ model output (original resolution 7x7 km<sup>2</sup>) and the ‘CHIMERE-SHERPA with QUARK applied’ model output (original grid resolution 125 x 125 m<sup>2</sup>, aggregated into the default mapping resolution of 1x1 km<sup>2</sup>) in the mapping. Although the CHIMERE-SHERPA model outputs are not suitable for the routine use in the mapping due to their limited domain with Iceland and large parts of Scandinavia missing, their mutually comparison shows the influence of the QUARK kernel method application, which could be in principle applied on another model output as well (including the routinely used EMEP).

Based on the comparison executed, it can be concluded that the application of QUARK method on the model used in the mapping does not lead to the improvement of the mapping results, at the presently used 1x1 km<sup>2</sup> resolution.

It must be noted however that the aggregation of the QUARK 125x125 m<sup>2</sup> model output to 1x1 km<sup>2</sup> largely flattens out the road-side gradients introduced by the kernel methodology. As such this operation to some extent defeats the purpose of this high resolution methodology.

### **Other potential developments**

Given the fact that the ETC/ACM maps are produced using the EMEP model output and new 10x10 km EMEP data is available at EU-scale, it could be an interesting option to couple the QUARK kernel methodology with the EMEP data. The advantage of the EMEP model output compared to the CHIMERE-SHERPA is that it covers the whole mapping domain including northern Scandinavia and Iceland.

Additionally to potential improvements of the ETC/ACM mapping as examined in this paper, an alternative method for coupling of the QUARK kernel method with the ETC/ACM mapping could be explored, i.e. applying the QUARK method on the ETC/ACM maps as background concentrations instead of the CHIMERE or EMEP model outputs. This alternative method is not directly in line with the current method, as it does not directly integrate the traffic (or, in one of its variants, even urban/suburban background) measurements. However, it aims at different applications than the current mapping, namely at the scenario calculations. For such a case, its advantage is in a coherence in mapping between ETC/ACM (and thus EEA) maps and DG – ENV policy tool.

For some purposes, it can be useful to refine the map resolution. For a potential refinement of the air quality maps into a 100x100 m<sup>2</sup> resolution, several approaches could be examined, including the ETC/ACM “regression – interpolation –merging” mapping using land cover in 100x100 m<sup>2</sup> resolution.

All the comparisons in this paper have been performed based on the concentration based statistics (using cross-validation). Next to this, it would be instructive to see the differences between the variants in term of population exposure, i.e. to calculate the population exposure based on different mapping variants and to compare these results. The same would apply also for all potential maps in 100x100 m<sup>2</sup> resolution.

## References

- Beelen R, Hoek G, Pebesma E, Vienneau D, de Hoogh K, Briggs D (2009). Mapping of background air pollution at a fine spatial scale across the European Union. *Science of the Total Environment* 407, 1852–1867. doi:10.1016/j.scitotenv.2008.11.048
- Beelen R, Hoek G, Vienneau D, Eeftens M et al. (2013). Development of NO<sub>2</sub> and NO<sub>x</sub> land use regression models for estimating air pollution exposure in 36 study areas in Europe – The ESCAPE project. *Atmospheric Environment* 72, 10–23.
- Bessagnet B, Terrnoire E, Tognet F, Rouil L, Colette A, Letinois L, Malherbe L (2012). EC4MACS Modelling Methodology - The CHIMERE Atmospheric Model. [http://www.ec4macs.eu/content/report/EC4MACS\\_Publications/MR\\_Final%20in%20pdf/Chimere\\_Methodologies\\_Final.pdf](http://www.ec4macs.eu/content/report/EC4MACS_Publications/MR_Final%20in%20pdf/Chimere_Methodologies_Final.pdf)
- Cressie N (1993). *Statistics for spatial data*. Wiley series, New York.
- Danielson JJ, Gesch DB (2011). Global multi-resolution terrain elevation data 2010 (GMTED2010): U.S. Geological Survey Open-File Report 2011–1073. <https://lta.cr.usgs.gov/GMTED2010>
- ECMWF (2015). Meteorological Archival and Retrieval System (MARS). <http://www.ecmwf.int/>
- EEA (2011). Guide for EEA map layout. EEA operational guidelines. August 2011, version 4. [http://www.eionet.europa.eu/gis/docs/GISguide\\_v4\\_EEA\\_Layout\\_for\\_map\\_production.pdf](http://www.eionet.europa.eu/gis/docs/GISguide_v4_EEA_Layout_for_map_production.pdf)
- EEA (2016a). Air Quality e-Reporting. Air quality database. <http://www.eea.europa.eu/data-and-maps/data/aqereporting-1>
- EEA (2016b). Corine land cover 2006 (CLC2006) raster data. 100x100m gridded version 18.5 (9/2016). <https://www.eea.europa.eu/data-and-maps/data/clc-2006-raster-4>
- EEA (2017). Air Quality e-Reporting. Air quality database. <http://www.eea.europa.eu/data-and-maps/data/aqereporting-2>
- EMEP (2012). Transboundary acidification, eutrophication and ground level ozone in Europe in 2010. EMEP Report 1/2012. [http://emep.int/publ/reports/2012/status\\_report\\_1\\_2012.pdf](http://emep.int/publ/reports/2012/status_report_1_2012.pdf)
- EMEP (2016). Transboundary particular matter, photo-oxidants, acidifying and eutrophying components. EMEP Status Report 1/2016. [http://emep.int/publ/reports/2016/EMEP\\_Status\\_Report\\_1\\_2016.pdf](http://emep.int/publ/reports/2016/EMEP_Status_Report_1_2016.pdf)
- Hoek, G., R. Beelen, K. de Hoogh, D. Vienneau, J. Gulliver, P. Fischer, and D. Briggs (2008), A review of land-use regression models to assess spatial variation of outdoor air pollution, *Atmos. Environ.*, 42(33), 7561–7578, doi:10.1016/j.atmosenv.2008.05.057.
- Horálek J, Denby B, de Smet P, de Leeuw F, Kurfürst P, Swart R, van Noije T (2007). Spatial mapping of air quality for European scale assessment. ETC/ACC Technical paper 2006/6. [http://acm.eionet.europa.eu/reports/ETCACC\\_TechPaper\\_2006\\_6\\_Spat\\_AQ](http://acm.eionet.europa.eu/reports/ETCACC_TechPaper_2006_6_Spat_AQ)
- Horálek J, de Smet P, de Leeuw F, Kurfürst P, Benešová N (2017a). European air quality maps for 2014. ETC/ACM Technical Paper 2016/6. [http://acm.eionet.europa.eu/reports/ETCACM\\_TP\\_2016\\_6\\_AQMaps2014](http://acm.eionet.europa.eu/reports/ETCACM_TP_2016_6_AQMaps2014)

Horálek J, de Smet P, Schneider P, Kurfürst P, de Leeuw F (2017b). Inclusion of land cover and traffic data in NO<sub>2</sub> mapping methodology. ETC/ACM Technical Paper 2016/12.

[http://acm.eionet.europa.eu/reports/ETCACM\\_TP\\_2016\\_12\\_LC\\_and\\_traffic\\_data\\_in\\_NO2\\_mapping](http://acm.eionet.europa.eu/reports/ETCACM_TP_2016_12_LC_and_traffic_data_in_NO2_mapping)

Horálek J, de Smet P, de Leeuw F, Kurfürst P (2017c). European NO<sub>2</sub> air quality map for 2014. Improved mapping methodology using land cover and traffic data. ETC/ACM Technical Paper 2017/6. [http://acm.eionet.europa.eu/reports/ETCACM\\_TP\\_2017\\_6\\_improved2014NO2\\_AQMap](http://acm.eionet.europa.eu/reports/ETCACM_TP_2017_6_improved2014NO2_AQMap)

Horálek J, de Smet P, de Leeuw F, Kurfürst P, Benešová N (2018). European air quality maps for 2015. ETC/ACM Technical Paper 2017/7.

[http://acm.eionet.europa.eu/reports/ETCACM\\_TP\\_2017\\_7\\_AQMaps2015](http://acm.eionet.europa.eu/reports/ETCACM_TP_2017_7_AQMaps2015)

JRC (2009). Population density disaggregated with Corine land cover 2000. 100x100 m grid resolution, EEA version popu01clcv5.tif of 24 Sep 2009. <http://www.eea.europa.eu/data-and-maps/data/population-density-disaggregated-with-corine-land-cover-2000-2>

Lefebvre W, Van Poppel M, Maiheu B, Janssen S, Dons E (2013). Evaluation of the RIO-IFDM-street canyon model chain. Atmospheric Environment 77, 325–337. doi:10.1016/j.atmosenv.2013.05.026

Mareckova K, Wankmüller R, Whiting R, Pinteris M (2012). Inventory Review 2012. Review of emission data reported under the LRTAP Convention and NEC Directive. Stage 1 and 2 Review. EEA/CEIP Technical Report.

[http://www.ceip.at/fileadmin/inhalte/emep/pdf/2012/InventoryReport2012\\_forWeb.pdf](http://www.ceip.at/fileadmin/inhalte/emep/pdf/2012/InventoryReport2012_forWeb.pdf)

Mareckova K, Pinterits M, Wankmüller R, Tista M (2016). Inventory Review 2016. Review of emission data reported under the LRTAP Convention and NEC Directive. Stage 1 and 2 review & Status of gridded and LPS data. EEA/CEIP Technical Report 1/2016.

[http://www.ceip.at/review\\_proces\\_intro/review\\_reports](http://www.ceip.at/review_proces_intro/review_reports)

Meijer JR, Huijbregts MAJ, Schotten CGJ, Schipper AM (2016). Mapping the global road network. Global Road Inventory Project (GRIP) of PBL.

[http://geoservice.pbl.nl/website/flexviewer/index.html?config=cfg/PBL\\_GRIP.xml&center=556597.6800125&scale=5000000](http://geoservice.pbl.nl/website/flexviewer/index.html?config=cfg/PBL_GRIP.xml&center=556597.6800125&scale=5000000)

NASA (2017). OMNO2d level 3 satellite data.

[https://acdisc.gsfc.nasa.gov/opensap/HDF-EOS5/Aura\\_OMI\\_Level3/OMNO2d.003/contents.html](https://acdisc.gsfc.nasa.gov/opensap/HDF-EOS5/Aura_OMI_Level3/OMNO2d.003/contents.html)

NILU (2016). EBAS, database of atmospheric chemical composition and physical properties (NILU, Norway). <http://ebas.nilu.no/>

NMI (2016). EMEP/MSC-W modelled air concentrations and depositions. Yearly, monthly, daily and hourly gridded data. [http://thredds.met.no/thredds/catalog/data/EMEP/2016\\_Reporting/catalog.html](http://thredds.met.no/thredds/catalog/data/EMEP/2016_Reporting/catalog.html)

ORNL (2008). ORNL LandScan high resolution global population data set.

[http://www.ornl.gov/sci/landscan/landscan\\_documentation.shtml](http://www.ornl.gov/sci/landscan/landscan_documentation.shtml)

Simpson D, Benedictow A, Berge H, Bergström R, Emberson LD, Fagerli H, Hayman GD, Gauss M, Jonson JE, Jenkin ME, Nyíri A, Richter C, Semeena VS, Tsyro S, Tuovinen J-P, Valdebenito A, Wind P (2012). The EMEP MSC-W chemical transport model – technical description. Atmospheric Chemistry and Physics, 12, 7825–7865, doi:10.5194/acp-12-7825-2012.

<http://www.atmos-chem-phys.net/12/7825/2012/acp-12-7825-2012.html>

Schneider P, Tarrasón L, Guerreiro C (2012). The potential of GMES satellite data for mapping nitrogen dioxide at the European scale, ETC/ACM Technical Paper 2012/9.

[acm.eionet.europa.eu/reports/ETCACM\\_TP\\_2012\\_9\\_GMESsatdata\\_NOx\\_Euromap](http://acm.eionet.europa.eu/reports/ETCACM_TP_2012_9_GMESsatdata_NOx_Euromap)

# Annex 1      **Overview of current and future satellite products of NO<sub>2</sub>**

As of end-2017 there are currently two major satellite instruments of relevance for the typical applications of the European spatially interpolated air quality mapping: OMI on the Aura platform and the GOME-2A/GOME-2B instruments onboard of the two MetOp platforms. In addition, the TROPOMI instrument onboard the Sentinel-5P platform has been launched in October 2017 and its data will be available at significantly higher spatial resolution and likely at higher accuracy.

In satellite remote sensing, various products are generated ranging from raw to highly processed data. The processing applied to each product is described using levels, generally ranging from Level-0 to Level-4. Whereas Level-0 (raw data) and Level-1 (calibrated raw data) are not too useful for the end users, Level-2 products provide the geophysical variable (e.g. tropospheric column of nitrogen dioxide), given at the same irregular geometry of the satellite overpass (i.e. spatially irregular observations). Level-3 are generally products that provide the same variables as Level-2 but mapped on a uniform space-time grid scale (e.g. a regular latitude/longitude grid). Finally, Level-4 products combine Level-3 with some additional model output or other data sources to create a value-added dataset.

Only Level-3 products are described here because of their general ease of use. Some more time-critical applications or comparisons with chemical transport models might require the use of swath-level products (Level-2).

## **A1.1 Ozone Monitoring Instrument (OMI)**

The Ozone Monitoring Instrument (OMI) is based on the experiences acquired from both GOME and SCIAMACHY [Levell *et al.*, 2006]. It combines their advantages, measuring the complete spectrum in the UV/VIS wavelength range at a comparatively high spatial resolution of 13 km x 24 km, while providing daily global coverage. The OMI instrument is flying on the National Aeronautics and Space Administration's Earth Observing System Aura platform as part of the A-train constellation of satellites. In contrast to the other instruments mentioned here, which have equator crossing times around 10:00 local time, OMI has an equator crossing time of approximately 1:45 LST in the afternoon, and therefore probes the Earth's atmosphere under different conditions. Aura/OMI was launched in 2004 and has been continuously providing data. Beginning in June 2007, OMI has suffered from several row anomalies affecting the quality of the Level 1B and Level 2 data products. Level-3 products are produced after filtering for the affected anomalies.

Two operational NO<sub>2</sub> products are available for OMI: (1) the one using the Dutch DOMINO algorithm (available at [temis.nl](http://temis.nl)) and (2) the one produced by NASA. It is recommended using the one provided by NASA, and in particular the OMNO2d product, which is easiest to work with. The reason for this is that the Dutch OMI product used a combined retrieval and assimilation approach in which some of the necessary retrieval information (i.e. the stratospheric part of the slant column) is obtained by assimilating the observations into a model and using the model output. While the DOMINO algorithm results in reliable NO<sub>2</sub> fields and has been validated thoroughly, for some applications it can be preferable to use a more “pure” satellite retrieval product that has not been previously assimilated into a model. Such a product is provided by NASA with its OMNO2 series of products, specifically the gridded Level-3 OMNO2d product. The actual OMNO2 product is Level-2 and provides swath-level retrievals of NO<sub>2</sub> and includes all pixels from all overpasses. In contrast, OMNO2G and OMNO2d are Level-3 products and provide gridded maps of NO<sub>2</sub> which only include a selection of the “best” retrievals filtered according to various criteria. The OMNO2d product [Bucsela *et al.*, 2006, 2013] is produced once per day using all available orbits for that particular day and provides an average value of the “best” pixels from the individual orbits.

The OMNO2d data product is a Level-3 Gridded Product where pixel level data of good quality are binned and "averaged" into 0.25x0.25 degree global grids. This product contains variables estimating *Total column NO<sub>2</sub>* and *Total Tropospheric Column NO<sub>2</sub>*, for all atmospheric conditions, and for sky conditions where cloud fraction is less than 30 percent. Details are available in the documents provided on the NASA GES DISC OMI site.

**Table A1.1 Description of NO<sub>2</sub> satellite data from OMI**

Parameter	Description
Product Name	OMNO2d
Frequency	Daily
Overpass time	ca. 13:30 LST
Processing Level	Level-3
Data Access	Through the various methods described at <a href="https://disc.gsfc.nasa.gov/datasets/OMNO2d_V003/summary">https://disc.gsfc.nasa.gov/datasets/OMNO2d_V003/summary</a>  A very simple method is to use the OPeNDAP service at: <a href="https://acdisc.gsfc.nasa.gov/opendap/HDF-EOS5/Aura_OMI_Level3/OMNO2d.003/contents.html">https://acdisc.gsfc.nasa.gov/opendap/HDF-EOS5/Aura_OMI_Level3/OMNO2d.003/contents.html</a>
Data Format	HDF5

## A1.2 GOME-2 onboard of the MetOp platform

The Global Ozone Monitoring Experiment-2 (GOME-2) is a scanning spectrometer onboard of the MetOp series of satellites. As a modified and improved successor of ERS-2's GOME instrument, GOME-2 measures in a spectral range of 240 nm to 790 nm with a varying spectral resolution between 0.24 nm and 0.53 nm [Callies *et al.*, 2000]. The spatial resolution of the instrument is 80 km x 40 km at nadir. There are two MetOP platforms, which each carry their own GOME-2 instrument: GOME-2A is located on MetOp-A and has been providing data since 2007. GOME-2B is located on MetOp-B and has been providing data since 2013.

**Table A1.2 Description of NO<sub>2</sub> satellite data from GOME-2**

Parameter	Description
Product Name	GOME2.L3.TropNO2.VCD.
Frequency	Daily
Overpass time	ca. 9:30 LST
Processing Level	Level-3
Data Access	DLR WDC-RSAT (World Data Center for Remote Sensing of the Atmosphere) <a href="http://wdc.dlr.de/data_products/SERVICES/GOME2NRT/no2tropo.php">http://wdc.dlr.de/data_products/SERVICES/GOME2NRT/no2tropo.php</a> and <a href="http://wdc.dlr.de/php/indexer_r.php?dir_index=1&amp;spec=TropNO2&amp;url=/data_products/SERVICES/GOME2NRT/archive.php">http://wdc.dlr.de/php/indexer_r.php?dir_index=1&amp;spec=TropNO2&amp;url=/data_products/SERVICES/GOME2NRT/archive.php</a> (Registration required)
Data Format	NetCDF

### **A1.3 TROPOMI onboard of the Sentinel-5P platform**

The TROPOMI instrument [Veefkind *et al.*, 2012] has been launched as the only payload of the Sentinel-5 Precursor mission, just 13 October 2017. The first test data for the TROPOMI validation team has been available in late 2017, while the operational data delivery is expected to start approximately in mid-2018. TROPOMI will provide NO<sub>2</sub> maps (and other species) at an unprecedented 7 km x 7 km spatial resolution while covering the entire Earth surface every day. As such it will be the primary instrument to be used in future.

### **A1.4 Use of NO<sub>2</sub> satellite data in Copernicus Atmosphere Monitoring Service (CAMS)**

The Copernicus Atmosphere Monitoring Service (CAMS) operates the regional and the global atmospheric environmental services.

#### **CAMS regional and ensemble system**

The regional service provides daily 4-day forecasts of the main air quality species, analyses of the day before from seven atmospheric chemistry models and from the median ENSEMBLE calculated from the seven models. The regional service also provides a reanalyses, using the latest validated observation dataset available for assimilation.

Seven models are interpolated on 0.1° x 0.1° grid over the European domain (25°W-45°E, 30°N-70°N). Those models are: CHIMERE (INERIS, France), EMEP (MET Norway), EURAD-IM (University of Cologne, Germany), LOTOS-EUROS (KNMI and TNO, Netherlands), MATCH (SMHI, Sweden), MOCAGE (METEO-FRANCE, France), SILAM (FMI, Finland). ENSEMBLE is currently based upon a median value approach. According to CAMS (2016), three models includes NO<sub>2</sub> satellite measurements in the data assimilation, namely

- EMEP – intermittent 3d-var assimilation, NO<sub>2</sub> columns from OMI;
- EURAD-IM – intermittent 3d-var assimilation, NO<sub>2</sub> column retrievals from AURA/OMI and METOP/GOME-2;
- SILAM – intermittent 3d-var assimilation, vertically integrated columns from OMI in research mode

#### **Global CAMS services**

CAMS produces global services in real-time (NRT system), in a delayed-mode configurations (DM system), and as a reanalysis (REA system). CAMS (2018) provides an overview of the satellite data use.

##### *Global real-time analysis and forecast system (NRT system)*

- uses satellite data in its 4-dimensional variational (4D-Var) data assimilation system to constrain the initial atmospheric state. NO<sub>2</sub> satellite measurements are used from OMI. Next to this, NO<sub>2</sub> satellite observations from the instrument TROPOMI of the satellite Sentinel-5p are being considered to be implemented in the CAMS system in near future.

##### *Global delayed-mode analysis and forecast system (DM system)*

- no satellite data for NO<sub>2</sub>, although it uses satellite data for other pollutants in its 4-dimensional variational (4D-Var) data assimilation system to constrain the initial atmospheric state.

### Global reanalysis (REA system)

- uses satellite data in its 4-dimensional variational (4D-Var) data assimilation system to constrain the atmospheric state every 6 hours. NO<sub>2</sub> satellite measurements are used from OMI and GOME-2.

## References

- Bucsela, E. J., E. A. Celarier, M. O. Wenig, J. F. Gleason, J. P. Veefkind, K. F. Boersma, and E. J. Brinksma (2006), Algorithm for NO<sub>2</sub> vertical column retrieval from the ozone monitoring instrument, *IEEE Trans. Geosci. Remote Sens.*, 44(5), 1245–1258, doi:10.1109/TGRS.2005.863715.
- Bucsela, E. J., N. a. Krotkov, E. a. Celarier, L. N. Lamsal, W. H. Swartz, P. K. Bhartia, K. F. Boersma, J. P. Veefkind, J. F. Gleason, and K. E. Pickering (2013), A new stratospheric and tropospheric NO<sub>2</sub> retrieval algorithm for nadir-viewing satellite instruments: applications to OMI, *Atmos. Meas. Tech.*, 6(10), 2607–2626, doi:10.5194/amt-6-2607-2013.
- Callies, J., E. Corpaccioli, M. Eisinger, A. Hahne, and A. Lefebvre (2000), GOME-2 - Metop's Second-Generation Sensor for Operational Ozone Monitoring, *ESA Bull.*, 102, 28–36.
- Levelt, P. F., G. H. J. van den Oord, M. R. Dobber, A. Malkki, P. Stammes, J. O. V. Lundell, and H. Saari (2006), The Ozone Monitoring Instrument, *IEEE Trans. Geosci. Remote Sens.*, 44(5), 1093–1101, doi:10.1109/TGRS.2006.872333.
- Veefkind, J. P. et al. (2012), TROPOMI on the ESA Sentinel-5 Precursor: A GMES mission for global observations of the atmospheric composition for climate, air quality and ozone layer applications, *Remote Sens. Environ.*, 120, 70–83, doi:10.1016/j.rse.2011.09.027.
- CAMS (2016). Regional Production, Description of the operational models and of the ENSEMBLE system. [https://atmosphere.copernicus.eu/sites/default/files/FileRepository/CAMS50\\_2015SC1\\_Models\\_Factsheet\\_201610\\_v2.pdf](https://atmosphere.copernicus.eu/sites/default/files/FileRepository/CAMS50_2015SC1_Models_Factsheet_201610_v2.pdf) (accessed 8.3. 2018)
- CAMS (2018). <https://atmosphere.copernicus.eu/cams-input-data> (accessed 20.3. 2018)

## Annex 2 QUARK kernel method and its potential integrating with ETC/ACM NO<sub>2</sub> mapping

In this annex we investigate the feasibility of the inclusion of the “QUARK (Quick Urban AiR quality using Kernels)” kernel method in EEA’s ETC/ACM mapping methodology. This kernel method has been derived by VITO in the recent DG-ENV project on improved tools for EU-wide NO<sub>2</sub> exposure assessment (070201/2015/SER/717473/C.3), see Maiheu et al. (2017). The aim of this is to explore and assess the feasibility of this coupling and discuss some specific points of attention.

In this note we first start with a brief description of the QUARK method, followed by a discussion on different ways of coupling or integrating this methodology with the current ETC/ACM “regression-interpolation-merging” mapping of NO<sub>2</sub>, which is primarily based on air quality measurements at monitoring stations and in which land use regression is included.

### A2.1 QUARK kernel methodology description

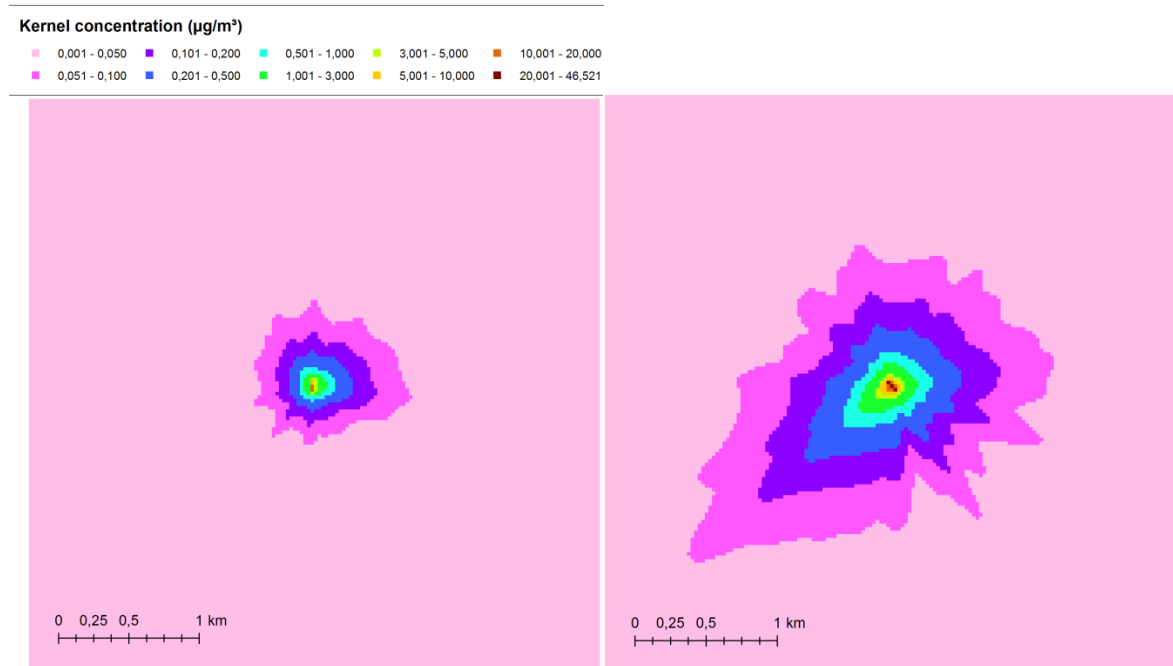
The methodology referenced in the title is based on a “bottom up” approach. Starting from coarse resolution background concentration grids (in which all relevant emissions are assumed to be represented), the concentration contributions from emissions for the sectors of interest (i.e. SNAP7, road traffic) are replaced by a higher resolution dispersion calculation, explicitly accounting for individual point or line emission sources. This method is described in detail in the scientific literature (Lefebvre et al., 2015, 2013, 2011).

The objective is to explicitly factor in traffic emissions (SNAP7), being the dominant source sector for NO<sub>2</sub> concentrations, at the level of line sources. Assuming that traffic emissions can be adequately attributed to line sources, air quality assessment usually uses local scale dispersion model, often based on Gaussian or Lagrangian modelling principles, to generate resulting concentration patterns. However, a complete hour-by-hour high resolution calculation using such a model is unfeasible at EU-scale. As we are mainly interested in the annual averaged concentration levels, a pre-existing database of dispersion patterns (kernels) for the roads having unit emission strength is generated. These kernels reflect the annual averaged dispersion characteristics in terms of specific parameters (wind speed, temperature, stability ...) at a specific location. Afterwards, the kernels are scaled with the particular emissions of the line source and each contribution is added to a map.

#### Kernels

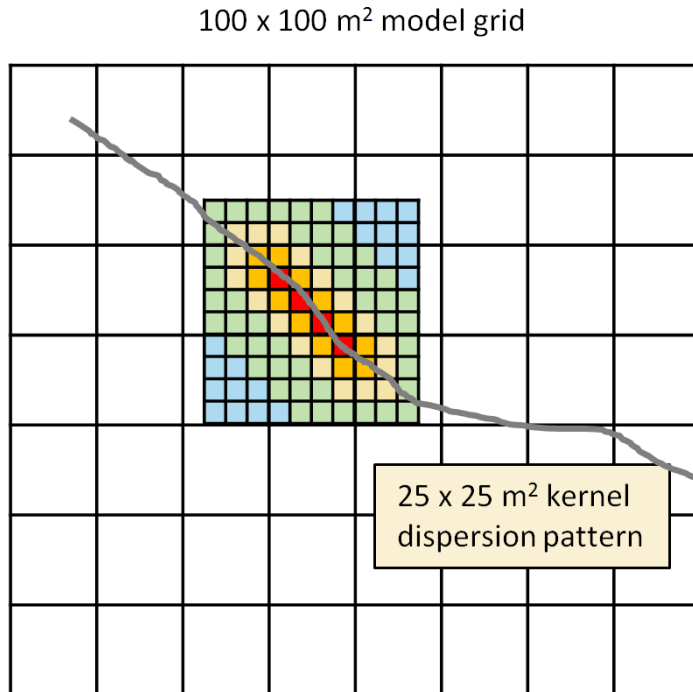
Dispersion kernels are annual averaged dispersion patterns of a single source (point source, line source,...) to which a unit emission strength is attributed. The calculation is typically performed by running a dispersion model hour-by-hour (e.g. Gaussian model such as IFDM used in Maiheu et al., 2017) with a meteorological dataset of a full year, generating different dispersion patterns (illustrated below, see Figure A2.1) depending on the local meteorology. The emissions are modulated with a temporal pattern representing the diurnal cycle of traffic emissions. The resulting concentration field is rasterized (on a grid of 25 x 25 m<sup>2</sup> in this case).

**Figure A2.1 Annual average dispersion kernel for a 100 m line source, of emission strength 1 kg/km/hour, at an angle of 5° from the North-South axis in the Northern part of Denmark (left), resp. at an angle of 135° from the North-South axis slightly north of Rome, Italy (right)**



For the line source (roads) dispersion kernels, segments of 100m length at varying angles from the North-South axis in steps of  $10^\circ$  (i.e. at 18 different angles) have been chosen. Based on analysis of the variability of the wind field (using ECMWF data for the year 2010), 5602 distinct (in terms of meteorology) sets of kernels have been produced. In some flat regions (such as Belgium-The Netherlands) less distinct kernels have been computed compared to e.g. mountainous regions, where the meteorology is much more variable. For each of the 5602 distinct regions, the annual mean  $\text{NO}_x$  concentration patterns belonging to the 18 standard sources, using a standard unit emission strength of 1 kg/km/h, have been calculated and are stored in a kernel database, for further upscaling with the actual emission of the line segment. The dispersion simulation for such a standard line source is performed for a square area of  $4 \times 4 \text{ km}^2$  with the source centre in the middle.  $4 \times 4 \text{ km}^2$  is taken as a distance at which the road contribution becomes negligible on top of the urban background. It is assumed that beyond the distance of 4 km the impact of an individual line segment of 100m can be neglected and is fully blended into the regional background. The kernels themselves are calculated at a resolution of  $25 \times 25 \text{ m}^2$ , see Figure A2.2. The IFDM (Immission Frequency Distribution Model), Gaussian dispersion model has been used to this end (Lefebvre et al., 2013, 2011).

**Figure A2.2** Illustration of the 25 x 25 m<sup>2</sup> resolution grid at which the kernels are effectively calculated, embedded in the 100 x 100 m<sup>2</sup> model grid. In grey an example road segment is shown. Note that the kernel itself actually normally extends to 4x4 km<sup>2</sup>.



The reference road database was constructed based on the open transport map dataset (<http://opentransportmap.info/>) where only roads larger or equal to *SecondClass* roads were taken into account. The SNAP 7 sector emissions are distributed along these line sources, so that the sum of the line source emissions for every 7x7 km<sup>2</sup> cell, is equal to the total for the SNAP 7 sector for that cell. The coarse resolution emission data was obtained from E. Pisoni (JRC) and is the same data used for the CHIMERE 7x7 km<sup>2</sup> runs which were performed for training the SHERPA model, developed by JRC<sup>4</sup>. The ‘road capacity\*length in grid cell’ was used as a proxy for this reallocation of emissions. Note that as a result of the methodology, the proxy is only used to spread emissions within the 7x7 km<sup>2</sup> emission cells, not in between different cells.

### Creation of the European-wide map

The generation of the EU-wide map follows the following steps. First, an EU wide high resolution grid at 125 x 125 m<sup>2</sup> is constructed. For each 125 x 125 m<sup>2</sup> grid cell, two variables are defined and initialized to 0. These variables will track the concentrations for NO<sub>x</sub> (C\_NO<sub>x</sub>) and for NO<sub>2</sub> (C\_NO<sub>2</sub>) as passive pollutants during the calculations.

The database of line sources as defined above is split into line segments of 100 m and according to its location and orientation each segment is connected to the specific kernel in the database. In the next step, for every of those road segments, the contribution of the corresponding kernel grid (4x4 km<sup>2</sup> at a

<sup>4</sup> <https://ec.europa.eu/jrc/en/news/sherpa-computational-model-better-air-quality-urban-areas>

25x25 m<sup>2</sup> resolution) towards the European grid is derived. A loop over the relevant 125 m grid cells is performed and for each of those grid cells C\_NO<sub>x</sub> and C\_NO<sub>2</sub> are calculated as follows (for all grid cells which receive a contribution of the line source under investigation):

$$C\_NO_x = C\_NO_x + E*kernel \quad (A2.1)$$

$$C\_NO_2 = C\_NO_2 + E*R*kernel \quad (A2.2)$$

Where *kernel* is an average over the 25m kernel cells that cover the 125x125m<sup>2</sup> grid cells, *E* is the emission of the line source in kg/km/hour, and *R* is the NO<sub>2</sub> over NO<sub>x</sub> emission ratio assigned to that segment. At the end of this procedure, the 2D-arrays C\_NO<sub>x</sub> and C\_NO<sub>2</sub> contain the concentrations of NO<sub>x</sub> and NO<sub>2</sub> as if both were passive pollutants (no chemistry at the moment) and if no background concentrations of NO<sub>x</sub> and NO<sub>2</sub> were present.

When adding this local increment as calculated above to the background concentrations, a double counting of emissions should be avoided. Double counting arises from the fact that traffic emissions are present both in the regional background as well as in the high resolution contribution. To avoid this double counting, we average the local contribution over the background cell and subtract this result from the background before adding the local contributions at high resolution. This methodology has been demonstrated in Lefebvre et al. (2011).

Up to here, no chemical interaction is taken into account between NO<sub>x</sub> and NO<sub>2</sub>. The latter one is the result of background contributions or directly emitted NO<sub>2</sub>. To account for the chemical equilibrium in the atmosphere a procedure similar to the one described in Düring et al. (2011) is followed, meaning that a chemical equilibrium between NO, O<sub>3</sub> and NO<sub>2</sub> at annual basis is imposed, with the equilibrium coefficient, dependant on meteorology and background O<sub>3</sub> concentrations, given by:

$$r_{jk} = \frac{[O_3][NO]}{[NO_2]}$$

where square brackets denote concentrations in mol/cm<sup>3</sup>. Both the amount of NO<sub>x</sub> and total oxidants O<sub>x</sub> (Clapp and Jenkin, 2001) at the local scale (denoted with subscript l, whereas background concentrations are denoted with subscript b) can be derived as:

$$[NO_x]_l = C\_NO_{x-t}$$

$$[O_x]_l = [O_3]_b + C\_NO_{2-t}$$

Note that in the last equation the background O<sub>3</sub> concentrations are used as these are the concentrations “before” the reaction. The subscript \_t refers to the total (background + local) concentrations. The final NO<sub>2</sub> concentrations are given by:

$$[NO_2]_f = \frac{(-b - \sqrt{D})}{2}$$

where

$$-b = [O_x]_l + [NO_x]_l + r_{jk}$$

$$\sqrt{D} = \sqrt{(-b)^2 - 4[O_x]_l[NO_x]_l}$$

## A2.2 Potential integration of the QUARK kernel method in the ETC/ACM mapping methodology

Here we discuss how the QUARK method may be integrated in the ETC/ACM mapping methodology.

### QUARK EU-wide NO<sub>2</sub> high resolution map as an additional proxy

The QUARK EU-wide NO<sub>2</sub> high resolution map may be used as an additional proxy in the ETC/ACM mapping spatial interpolation scheme, as examined in Chapter 4 for 2010 data of ‘CHIMERE-SHERPA model with QUARK applied’. Below we discuss some of the advantages and disadvantages of this method, see Table A2.1.

**Table A2.1 Advantages and disadvantages of ‘QUARK high resolution map integration in the ETC/ACM mapping as an additional proxy’**

Method	Advantages	Disadvantages
<b>QUARK high resolution map as an additional proxy</b>	<ul style="list-style-type: none"> <li>• Methodology in line with the current mapping methodology for the ETC.</li> <li>• Simplicity of integration, maps are used only as a proxy in the LUR part of the ETC/ACM approach. QUARK maps generated offline.</li> <li>• Unbiased estimation: the method starts from measurements for the mapping</li> </ul>	<ul style="list-style-type: none"> <li>• The current LUR model already captures quite some of the spatial variability and includes information on the roads. Adding the QUARK map in the model essentially tests for its ability to predict the residuals from the current model, which may largely be statistical noise.</li> <li>• Spatial scale of the QUARK map is blurred by other proxies, even though the concentration increment is directly related to the emission contribution for the relevant sector.</li> <li>• When the QUARK map is resampled to 1km resolution, much of the variation in the QUARK map is lost.</li> </ul>

In general, this method poses no additional methodological challenges. The GIS map layer for 2010, which is available in EPSG3035 at 125 m resolution, was tested as an additional proxy (see main document). Since in the current multiple regression (resp. LUR) a large part of the spatial variability is taken away by the current proxy parameters, it is unclear to what extent the addition of the QUARK map would explain out of the box more spatial variability of the NO<sub>2</sub> field in Europe, in addition to what is already captured by the correlation of the measurements to the current LUR.

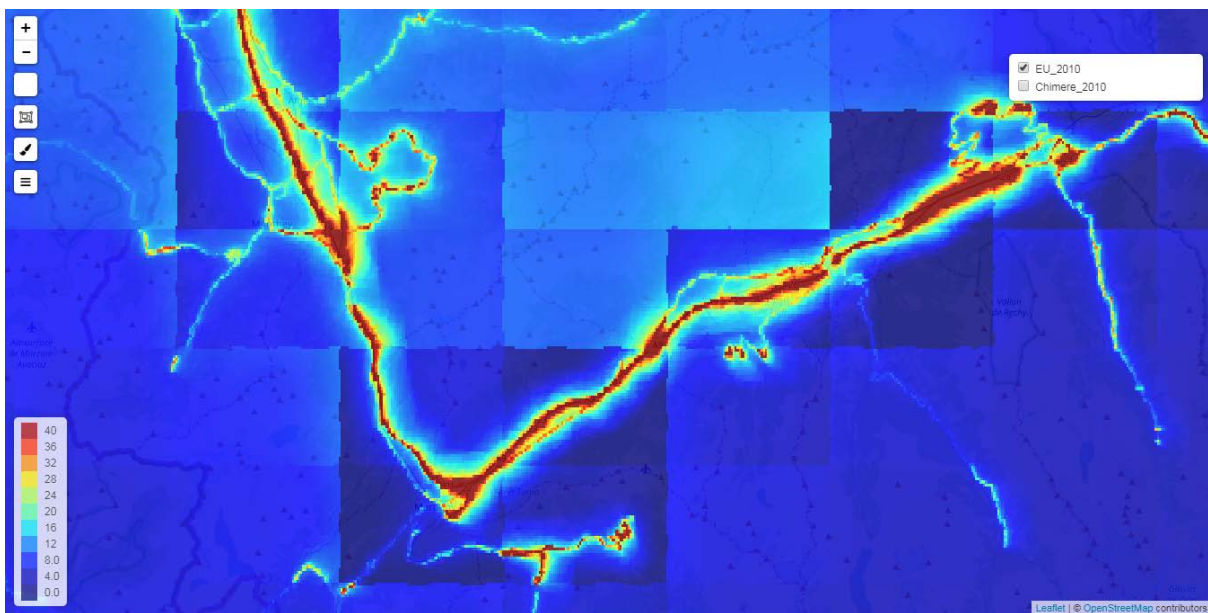
A number of improvements however are possible, which we will discuss briefly here.

- Currently the QUARK model uses CHIMERE background concentrations, from which it effectively needs the NO<sub>x</sub> total, NO<sub>2</sub> and O<sub>3</sub> annual averages. Given the recent availability of EMEP 0.1° results (10 km), it may be an interesting option to explore coupling the QUARK downscaling methodology to the EMEP model and test this as a proxy in the ETC/ACM mapping methodology. The advantages would be that the EMEP model has data for the northern part of Scandinavia and for Iceland as well, contrary to the CHIMERE domain, as well as provides the necessary pollutant fields for the QUARK methodology to be used “as is”. A coupling to EMEP would however require a re-generation of the traffic emission databases on the road segments to match with the coarse resolution emissions used in the EMEP 0.1° grid.
- Regarding the emission redistribution, an area where significant progress can be made would be the generation of a traffic emission redistribution at road segment level using OpenStreetMap/OpenTransportMap data. The redistribution of traffic emissions within the 7x7 km grid cells currently uses road capacity as derived from the OpenTransportMap project

data. Further investigations into this redistribution, taking observations from traffic stations into account has the potential of improving the spatial correlation of the mapping.

- Expansion of the kernels to national / regional level would be an interesting investigation to reduce the number of artefacts in the QUARK mapping methodology. A number of artefacts are present in the QUARK high resolution maps showing the underlying background concentration grid cell boundaries. Figure A2.3 illustrates this, showing the underlying CHIMERE 7x7 km<sup>2</sup> pattern and rather sharp jumps in concentration between these grid cells. The artefacts are the result of the double counting correction methodology and traffic emission redistribution inside the 7x7 km<sup>2</sup> grid cells. Since there is a difference in dispersion calculation between the kernel methodology and the CHIMERE model, the subtraction step at 7x7 km<sup>2</sup> in the background correction subtracts the averaged local scale traffic contribution, which may not completely match with the original CHIMERE 7x7 km<sup>2</sup> traffic contribution (due to the different dispersion methodology). Therefore, some jumps at the CHIMERE grid cell boundaries may be seen. These effects are not very substantial, however they do appear in the maps and are clearly visible in a similar way as other artefacts appear in the current ETC/ACM regression-interpolation-merging maps (connected to the EMEP coarse resolution pattern).

**Figure A2.3 Some artefacts visible in the QUARK model coupled with the CHIMERE background concentrations**



A possible solution for reducing these artefacts could be the generation of dispersion patterns which span a whole region/country, taking into account the road network of the whole area as well as traffic emission redistribution factors. This would have to be combined with an interpolation scheme for the background concentrations. The additional benefit of having such region-wide dispersion patterns is that they would directly link to country/region based emission totals used in EU-wide integrated scenario assessments as well as greatly reducing the computation time required. Artefacts such as the ones visible above would in this case be restricted largely to the country/region borders.

### A2.3 Potential alternative coupling of the QUARK kernel method with the ETC/ACM mapping methodology

Next to the approach discussed in Section A2.2, there is a second way of integrating the QUARK methodology with the ETC/ACM mapping, which is to use the *ETC/ACM maps as background concentrations instead of e.g. the CHIMERE or EMEP maps*. We mention here this alternative approach additionally, going beyond the basic scope of this paper, i.e. improvements of the current ETC/ACM method for mapping the NO<sub>2</sub> concentrations. Even though this method is not directly in line with the current ETC/ACM approach, which is solely based on regression and interpolation of its residuals, this method may offer some interesting potential use cases such that, in our opinion, it deserves some attention here. Clearly this method is directly relevant for EU policy road traffic scenario assessment and the formulation of air quality abatement plans. Furthermore, some of the research questions associated with the investigation into this method would directly benefit also method discussed in Section A2.2. Table A2.2 summarizes advantages and disadvantages of this method.

**Table A2.2 Advantages and disadvantages of ‘ETC/ACM maps as background concentrations instead of e.g. the CHIMERE or EMEP maps’**

Method	Advantages	Disadvantages
<b>ETC/ACM maps as background concentrations instead of e.g. the CHIMERE or EMEP maps</b>	<ul style="list-style-type: none"> <li>• Clearer contribution of the downscaled sectors, the rest is in background (LUR): spatial pattern more directly related to the emissions.</li> <li>• Dispersion patterns around key emission sources (traffic) may be more realistic</li> <li>• Allow for traffic scenario calculations</li> <li>• Coherence in mapping between: EEA maps and DG – ENV policy tool</li> </ul>	<ul style="list-style-type: none"> <li>• More involved and computationally intense (though feasible as demonstrated by DG-ENV project)</li> <li>• Needs to overcome some challenges → research questions</li> <li>• No direct integration of traffic measurements</li> <li>• No direct integration of urban/suburban background measurements, if spatially aggregated 10x10 km ETC/ACM maps are used</li> </ul>

As was mentioned above, the usage of land use regression models as background concentrations for an urban dispersion modelling has been well documented and is frequently being applied in concrete EIA’s (Lefebvre et al., 2013). Such a method would capture the background concentrations well by deriving them from representative in-situ observations, but add the local, inner-city variability directly from traffic emission source dispersion modelling. This very local variability would essentially be difficult to capture by using the available monitoring data alone as the abundance of traffic monitoring sites is limited.

It has to be noted that this type of model chain: a LUR based approach for the regional background in combination with a deterministic approach for the local sources is used both in the UK (PCM, see DEFRA, 2015) and in Belgium (RIO-IFDM, see Lefebvre et al., 2013) for official assessment maps. Major argument for such a hybrid approach is that concentration changes at the local scale are driven by local emission and local meteorology. Since in most regions only a handful of traffic stations are available to calibrate this contribution, it might be more accurate to rely on a deterministic approach than on a statistical one.

Furthermore, with LUR models, there is a real danger of overfitting in case of limited number of measurements, representing a certain spatial scale. At EU-level, there is likely an adequate amount of background monitoring stations to capture the spatial variation at urban background level, however the

amount of individual traffic stations within any given urban environment is maybe too limited to be able to calibrate the regression weights for proxies related to local road side increments. It was also shown that the inclusion of dispersion-like regression proxies significantly improves the LUR prediction modeling, however requiring several observation locations for each city to avoid overfitting (TRANSPHORM, 2010).

In addition one has to be careful in comparing the obtained spatial  $R^2$  from a leaving one out cross validation. Even though in a cross validation the monitoring data is not taken into account in the interpolation of the residual, it is the monitoring data which determines what predictor variables should be used. This is why there is a natural tendency in LUR models for better spatial correlation with the monitoring sites.

Clearly, there are a number of more challenging research questions involved, but also a number of interesting remarks to make here:

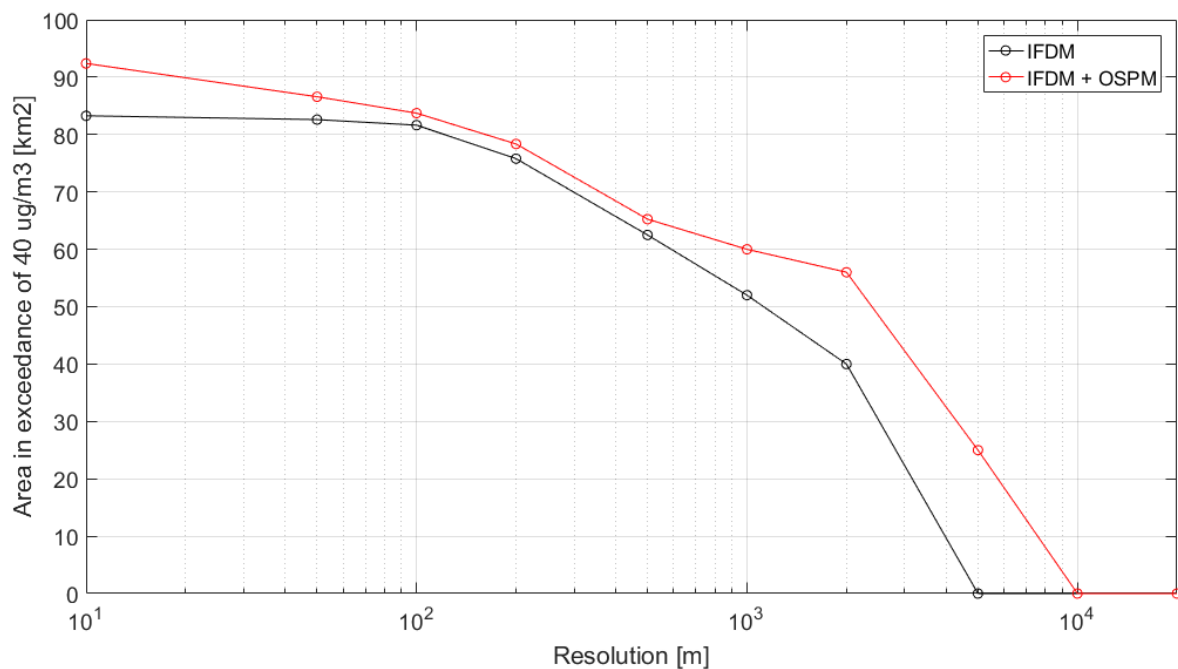
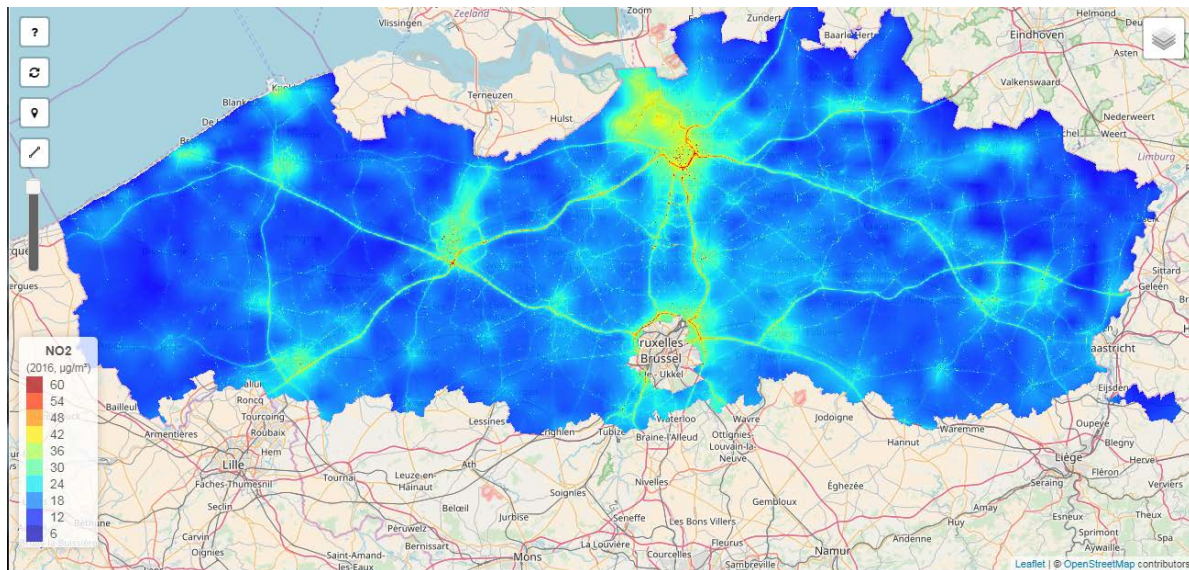
- During the DG-ENV service contract, the kernel methodology was established using the CHIMERE 7x7 km<sup>2</sup> background concentrations to start from. This in essence means that the background concentrations are averaged concentrations for the lowest model layer (typically ~10 m high). The coupling therefore requires some way of taking this vertical distribution of the concentrations into account when downscaling to a 2 m concentration map, or at least an assessment of the sensitivity of the final map with respect to this (as was done in the NO<sub>2</sub> exposure project). As the ETC/ACM mapping directly starts from surface level concentration measurements, the final ETC/ACM assessment maps can be considered as representative for the surface level (albeit at coarse resolution) and no correction for the vertical distribution of concentrations should be required.
- On the other hand, an interesting issue emerges regarding the emission double counting. When coupling the kernel methodology with CTM output, there is a clear need for an emission double counting correction as all the emissions are assumed present in the CTM background concentrations (albeit at lower resolution). However, when coupling with a LUR model, it is not entirely clear how to treat this double counting. It has to be investigated how well the ETC/ACM maps (be it the 1x1 km or the spatially aggregated 10x10 km versions) allow to capture the urban background and to what extent a double counting would be required (rather than a simple addition of the local traffic increment for NO<sub>2</sub>). An alternative would be to use the ETC/ACM background map layers, i.e. the maps without inclusion of the urban traffic layer.
- The chemical balance between NO<sub>2</sub>, O<sub>3</sub>, NO, is clear in chemical transport models. However, as the ETC/ACM maps are generated independently from each other, there is no connection between the different pollutant maps in terms of chemistry. This is e.g. reflected in the absence of lower O<sub>3</sub> concentration in urban environments (with high NO<sub>x</sub>) in VOC limited regions. Increased methodological consistency between the O<sub>3</sub> and NO<sub>2</sub> mapping could be a valuable addition.

#### **A2.4 Discussion on the spatial resolution and its influence on the exposure assessment**

The fitness for purpose of air quality assessments is an emerging topic which receives more and more attention, especially also within the frame of the FAIRMODE initiative. As a general principle, the spatial scale of an air quality assessment should be able to capture the spatial variability of the physical field it aims to represent. Large scale CTM-based assessments are for example not suited to assess concentrations inside street canyons as they cannot represent the spatial variability to that scale. Clearly, given the nature of dominant emission sources for NO<sub>2</sub>, the spatial variability is very high as illustrated by the map for Flanders below. We see that an assessment of the total area of exceedance strongly depends on the spatial resolution of the assessment (which was approximated by simple averaging of the NO<sub>2</sub> concentration field). At a scale of 1 km we obtain only about 60 % of the total

area in exceedance of the  $40 \mu\text{g}/\text{m}^3$  standard compared to what we obtain when taking the full resolution result into account.

**Figure A2.4** Illustration of the total area in exceedance of the  $40 \mu\text{g}/\text{m}^3$  for a high resolution model assessment for Flanders (using the IFDM+OSPM model chain, (Lefebvre et al., 2013)) at different spatial scales. The IFDM model only contains the road contributions, the IFDM+OSPM chain adds the street canyon increment as well. It can be seen that at 1 km resolution, the model only captures about 60% of the total area in exceedance which would be obtained by a full resolution assessment.



It should be noted that for population exposure purposes, it was shown in the DG-ENV project<sup>5</sup>, that the spatial scale at high resolution (< 1 km) is not such a dominant source of uncertainty, given the current population datasets (for which the scale is also only of the order of 1 km). And hence an exposure assessment at 1 km spatial scale would be sufficiently fine. However, given a number of caveats regarding the sensitivity analysis in that report and the stronger dependence on spatial resolution in the presence of a cut-off, a spatial scale of 100 m was recommended for EU-wide NO<sub>2</sub> exposure assessment.

It should be clear therefore that a higher spatial resolution than 1 km would be required especially around roads and strong point-sources to accurately capture the strong spatial gradients around the roads and hence provide for an accurate exceedance estimation. Special attention with respect to the street canyon increment in urban environments is required here, also in order to fully capture the spatial variability of NO<sub>2</sub> concentrations inside cities.

For reaching such a finer spatial scale, different approaches may be considered. In a context of the ETC/ACM mapping, a relevant approach could be the ETC/ACM mapping in 100 m resolution, using land cover data in 100 m resolution as a proxy; other proxy could be a downscaled model. In this context, the coupling of the QUARK downscaling methodology to the EMEP model as described in Section A2.2 could be relevant. An alternative approach could be the coupling of the QUARK method with the ETC/ACM mapping methodology as described in Section A2.3. Another potential methodology is geostatistical downscaling using techniques such as area-to-point kriging (Kyriakidis 2004, Park, 2013). The SAMIRA project (<http://samira.nilu.no>) funded by the European Space Agency is currently exploring such methods for downscaling satellite data of air quality (Schneider et al., 2017).

## **A2.5 Potential research questions list**

In light of the previous discussion, we briefly state here a list of priorities for a potential research plan regarding the integration of the QUARK methodology in the ETC/ACM mapping for NO<sub>2</sub> and other issues discussed in this Annex 2. Clearly, to be in line with the current methodology of mapping, there may be a preference towards using the QUARK map as an additional proxy in the LUR. However, there are some synergies between both methods introduced in Sections A2.2 and A2.3, in the sense that particular research questions would advance the application of the QUARK model for both methods. These should be given priority. Concerning the below stated list, it should be mentioned that it is related to the issues discussed in this Annex 2 only.

1. First and foremost, the road line-source data base determines to a large extent the spatial variability the QUARK model is able to capture with respect to the urban / traffic station concentrations. This would directly improve the spatial correlation of the LUR model (method discussed in Section A2.2), but would also benefit the application of the model in a scenario context (method discussed in Section A2.3). This could be attempted by extending the road network database (e.g. northern Scandinavia) and investigating if better proxies are available for the traffic intensity than the one that have been used until now. This investigation would include some optimization using information from traffic stations.
2. Given the fact that the ETC/ACM maps are produced using the EMEP data and new 10x10 km EMEP data is available at EU-scale, it could be an interesting option to couple the QUARK methodology to the EMEP data, analyzing the redistribution of the traffic emissions as well as the occurrence of artefacts.

---

<sup>5</sup> EC, DG-ENV Service Contract 070201/2015/SER/717473/C.3

3. Given the spatial variability of NO<sub>2</sub> concentrations, the impact of a higher resolution than 1 km could be further researched based upon the QUARK maps at 100 m resolution. It was shown that the total area in exceedance depends significantly on the spatial resolution (see Figure A2.4). It would be instructive to repeat the analysis presented for Flanders at the European scale.
4. For the ETC/ACM maps it was shown that the spatially aggregated 10x10 km data shows a bias for the urban background stations, whereas the 1x1 km does not. It would be interesting to investigate whether the kernel method could effectively resolve this bias when comparing to the measurements.
5. Researching a methodology to ensure consistency between the O<sub>3</sub> and NO<sub>2</sub> as far as the chemistry is concerned could be a valuable addition to the mapping regarding a potential use of the maps based on the method of Section A2.3 in scenario calculations.
6. For a potential refinement of the air quality maps into a 100x100 m resolution, several approaches could be examined, including the ETC/ACM mapping using land cover in 100 m resolution.

## References

- Bessagnet, B., Terrnoire, E., Tognet, F., Rouil, L., Colette, A., Letinois, L., Malherbe, L., 2012. EC4MACS Modelling Methodology - The CHIMERE Atmospheric Model.
- Clap, L.J., Jenkin, M.E., 2011. Analysis of the Relationship between ambient levels of O<sub>3</sub>, NO<sub>2</sub> and NO as a function of NO<sub>x</sub> in the UK. *Atmos. Environ.* 35, 6391–6405. doi:10.4209/aaqr.2010.07.0055
- DEFRA, 2015. Improving air quality in the UK Tackling nitrogen dioxide in our towns and cities - Technical report. Available at [https://www.gov.uk/government/uploads/system/uploads/attachment\\_data/file/492901/aq-plan-2015-technical-report.pdf](https://www.gov.uk/government/uploads/system/uploads/attachment_data/file/492901/aq-plan-2015-technical-report.pdf).
- Düring, I., Bächlin, W., Ketzler, M., Baum, A., Friedrich, U., Wurzler, S., 2011. A new simplified NO/NO<sub>2</sub> conversion model under consideration of direct NO<sub>2</sub>-emissions. *Meteorol. Zeitschrift* 20, 67–73. doi:10.1127/0941-2948/2011/0491
- Kyriakidis, P. C. (2004). A Geostatistical Framework for Area-to-Point Spatial Interpolation. *Geographical Analysis*, 36(3), 259–289. Available at <https://doi.org/10.1353/geo.2004.0009>.
- Lefebvre, W., Maiheu, B., Vranckx, S., Janssen, S., 2015. Development of a Screening Tool for Quick Environmental Assessment of Mobility Scenarios, in: International Technical Meeting on Air Pollution Modelling and Its Applications (ITM34). Montpellier, pp. 1–4.
- Lefebvre, W., Van Poppel, M., Maiheu, B., Janssen, S., Dons, E., 2013. Evaluation of the RIO-IFDM-street canyon model chain. *Atmos. Environ.* 77, 325–337. doi:10.1016/j.atmosenv.2013.05.026
- Lefebvre, W., Vercauteren, J., Schrooten, L., Janssen, S., Degraeuwe, B., Maenhaut, W., de Vlioger, I., Vankerkom, J., Cosemans, G., Mensink, C., Veldeman, N., Deutsch, F., Van Looy, S., Peelaerts, W., Lefebvre, F., 2011. Validation of the MIMOSA-AURORA-IFDM model chain for policy support: Modeling concentrations of elemental carbon in Flanders. *Atmos. Environ.* 45, 6705–6713. doi:10.1016/j.atmosenv.2011.08.033
- Maiheu, B., Lefebvre, W., Walton, H., Dajnak, D., Janssen, S., Williams, M., Blyth, L., Beevers, S. (2017). Improved Methodologies for NO<sub>2</sub> Exposure Assessment in the EU. Final report of service contract 070201/2015/SER/717473/C.3 for the European Commission, DG-Environment. Available at <http://ec.europa.eu/environment/air/pdf/NO2%20exposure%20final%20report.pdf>.
- Park, N.-W. (2013). Spatial Downscaling of TRMM Precipitation Using Geostatistics and Fine Scale Environmental Variables. *Advances in Meteorology* 11, Article ID 237126. doi:

10.1155/2013/237126

Schneider, P., Stebel, K., Ajtai, N., Diamandi, A., Horalek, J., Nemuc, A., Stachlewska, I., & Zehner, C. (2017). The Satellite based Monitoring Initiative for Regional Air quality (SAMIRA): Project summary and first results. *Geophysical Research Abstracts*, 19, EGU2017-3510.

TRANSPHORM, 2010. Transport related Air Pollution and Health impacts - Integrated Methodologies for Assessing Particulate Matter - Deliverable 2.4.1 - Report on the enhanced resolution and sub-grid downscaling of transport emissions. Available at [http://www.transphorm.eu/Portals/51/Documents/Deliverables/New\\_Deliverables/D2.4.1.pdf](http://www.transphorm.eu/Portals/51/Documents/Deliverables/New_Deliverables/D2.4.1.pdf).